Journal of Marine Research, 64, 589–627, 2006

Bio-irrigation in permeable sediments: An assessment of model complexity

by Filip J. R. Meysman[1,2], Oleksiy S. Galaktionov[1], Britta Gribsholt[1] and Jack J. Middelburg[1]

ABSTRACT

Burrowing benthic animals ventilate their burrow networks, and this enhances the transport of solutes in the sediment and exchange with the overlying water column, a process referred to as bio-irrigation. Various models have been proposed to model bio-irrigation, with different levels of sophistication related to model dimensionality and parameter numbers. Here we address the issue of model complexity for bio-irrigation in permeable sediments. To this end, we simulated flowline patterns and tracer signals using (1) a full 3D model that explicitly models the J-shaped geometry of the burrow in a suitable microenvironment surrounding the burrow, (2) a simplified 2D axi-symmetric analogue, which neglects the burrow shaft and only models the location of burrow water injection, (3) a highly simplified 1D model obtained by laterally averaging the microenvironment. Simulation of two separate inert tracer experiments shows that the 2D pocket injection model includes essential features (downward advective transport, spatial heterogeneity of pore water velocity, mechanistic specification of the seepage area) that are lost upon averaging to the corresponding 1D model. This loss of model detail must be compensated for by the introduction of additional, non-mechanistic fitting parameters in the 1D description. Similarly, the extension of the 2D model to a full sophisticated 3D description requires a major increase in computational resources, but only leads to a marginal improvement in the data simulation. Accordingly, we conclude that the 2D description provides an optimal balance between model simplicity and predictive capacity.

1. Introduction

Benthic macrofauna create burrows or burrow networks that penetrate deeply into the anoxic zone of the sediment (Anderson and Meadows, 1978). To sustain an aerobic metabolism, macrofauna flush their burrows with oxygen-rich water from the overlying water column, a process referred to as *burrow ventilation* (Gust and Harrison, 1981; Webb and Eyre, 2004). This burrow ventilation has a significant impact on the sediment, as it forms the driving force for *bio-irrigation*, the enhanced transport of solutes in the surroundings of the burrows (Rhoads, 1974). Bio-irrigation strongly influences sediment biogeochemistry (Davis, 1974; Aller and Aller, 1998; Wenzhöfer and Glud, 2004),

1. Centre for Estuarine and Marine Ecology, The Netherlands Institute of Ecology (NIOO-KNAW), Korringaweg 7, 4401 NT Yerseke, The Netherlands.
2. Corresponding author. ***email: f.meysman@nioo.knaw.nl***

microbial ecology (Hylleberg, 1975; Reichardt, 1988; Marinelli *et al.*, 2002), and solute exchange across the sediment-water interface (Christensen *et al.*, 1984; Archer and Devol, 1992; Meile and Van Cappellen, 2003). To assess these various impacts, one requires a thorough quantitative understanding of bio-irrigation, which crucially depends on an accurate mathematical model description (Aller, 2001).

A "model" constitutes by definition an idealized and simplified representation of reality. Therefore, a central question in model development is that of model complexity: how simplified can a model be and still describe the natural system adequately? On this topic, Albert Einstein once made the famous quote that "things should be made as simple as possible, but not simpler than that." Here we address the issue of model complexity in the context of bio-irrigation. The bio-irrigated zone is a complex three-dimensional (3D) mosaic of biogenic structures. Therefore, a number of questions arise when "harnessing" this zone in an idealized model representation. Does the inherent 3D nature of bio-irrigated zone necessarily imply that we also need models with the same sophistication and complexity? Or can we still use simplified one-dimensional (1D) formulations, and if not, when and why do 1D models fail? How do idealizations affect the mechanistic basis and predictive capacity of bio-irrigation models? In other words, we need to examine to what level the daunting complexity of the bio-irrigated zone can be simplified, while still retaining the fundamental characteristics of the bio-irrigation process.

One elegant way to construct mechanistic bio-irrigation models is by defining a representative micro-environment that incorporates an idealized burrow geometry (Aller, 1980, 2001). Such micro-environment models idealize bio-irrigated sediments as a collection of separate "territories" or burrow units, each inhabited by a single burrowing organism. 1D and 2D formulations are then obtained by properly simplifying and/or averaging the original 3D micro-environment. Up to present, two main types of micro-environment models have been proposed: the diffusive tube-irrigation model (Aller, 1980) and the advective pocket-injection model (Meysman *et al.*, 2006). These models describe bio-irrigation in respectively muds and sands, via two end-member links between burrow ventilation and bio-irrigation.

In muds, bio-irrigation is intrinsically driven by diffusion across the burrow wall. To describe this "diffusive" mechanism, Aller (1980) proposed the tube-irrigation micro-environment model, which formed a true milestone in the quantitative approach to bio-irrigation. This model assumes that (1) a territory is a cylindrical domain with a central cylindrical void representing the burrow, (2) the organism vigorously mixes the burrow water so that its composition always equals that of the overlying water, and (3) the actual process of bio-irrigation is caused by radial diffusion of solutes from the burrow water through the burrow wall into the surrounding sediment. Because of radial symmetry, the 3D micro-environment can be described using a 2D mathematical model formulation. Over the years, extensions have been proposed that relax some of the idealizations of Aller's original 2D model. Boudreau and Marinelli (1994) investigated how periodic, discontinuous ventilation of burrows affects burrow water composition and sediment biogeochemis-

try. Furukawa *et al.* (2001) extended the model to burrows that have a depth dependent radius and tilt angle. Koretsky *et al.* (2002) applied the model to stochastic realizations of 3D burrow networks. In a similar fashion, possible simplifications to 1D have been examined. Boudreau (1984) showed how lateral averaging of the tube-irrigation model can result in the conventional non-local exchange description. Recently, Grigg *et al.* (2005) and Meile *et al.* (2005) further examined the relation between the 2D model and the laterally averaged 1D version.

In sandy sediments, the mechanism of bio-irrigation can be rather different from that in muddy environments. Due to the higher permeability, organisms can actively pump water across the burrow wall when ventilating their burrows (Foster-Smith, 1978). These flows will penetrate the sediment surrounding the burrow and induce pore water advection. To model the impact of such biologically induced flows, Meysman *et al.* (2006) have recently proposed the 2D pocket-injection model. This micro-environment model can be regarded the "advective" counterpart of the Aller (1980) "diffusive" model. The principal features of the 2D pocket-injection model are that (1) organisms indent the sediment-water interface with burrows that blindly end into an injection pocket with a highly permeable lining, (2) burrow water is injected from the injection pocket into the sediment, and (3) the actual process of bio-irrigation is caused by the resulting flow in the surrounding pore water.

Overall, one could say that there is a reasonable body of work on the complexity of bio-irrigation models for muddy environments, based on the study of Aller's original tube-irrigation model and subsequent extensions. The aim of this work is to systematically investigate the required complexity of bio-irrigation models in sandy sediments. This is done in a detailed case study of the advective bio-irrigation induced by burrow ventilation of the lugworm *Arenicola marina.* Velocity and concentration patterns are compared for 1D, 2D and 3D models of the environment surrounding the lugworm's burrow. To assess the predictive capabilities of the individual models, the simulation results are compared to data obtained from laboratory experiments with inert tracers.

2. Material and methods

a. Modeling approach

We selected *Arenicola marina* as study object because lugworms constitute a dominant type of bio-irrigators in temperate near-shore sandy environments (Cadée, 1976; Beukema and Vlas, 1979; Reise, 1985). A substantial amount of background information on its pumping behaviour has been gathered in the past (see review by Riisgård and Banta, 1998). *A. marina* dwells in J-shaped burrows, and generates a water flow by means of piston-like waves that run along its dorsal surface (Kruger, 1971). When pumping, the worm resides in the lower horizontal part of the burrow called the "gallery." The suction created by peristaltic motions takes in oxygenated water from the overlying water column. Passing through the burrow and over the lugworm's gills, this water is subsequently pumped through the porous walls of the feeding pocket into the surrounding sediment (Fig. 1a).

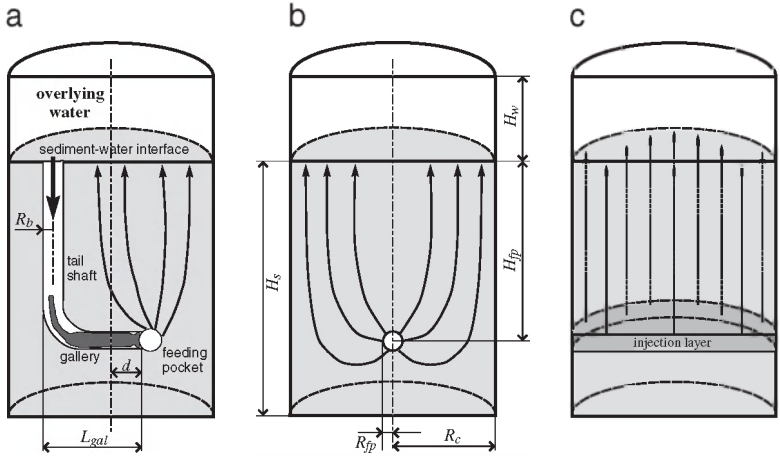

Figure 1. Various degree of spatial complexity in describing a typical lugworm territory. This domain either represents an *in-situ* micro-environment or a laboratory set-up. (a) Full 3D model description of a cylindrical domain with J-shaped burrow. (b) 2D axi-symmetric model with only a feeding pocket. (c) 1D model with localized injection.

This creates an advective transport of pore water back to the sediment surface. Passing through the sediment, this return flow will in general attain a different composition as the water that enters the burrow, and hence, it will affect the composition of the overlying water.

To quantify the impact of lugworm bio-irrigation on sediment biogeochemistry, we employ models that each consist of three separate subunits (Table 1 provides a list of symbols). In a first step, we simulate the velocity pattern that is induced in the pore water by the lugworm's pumping. This model is termed the flow model (FM) and is based on the principle of momentum conservation. In a second step, the calculated pore water velocity is incorporated in the mass conservation equation of a particular solute. This model is termed the transport model (TM) and predicts the tracer's concentration distribution within the sediment. In a third step, we describe the compositional changes in the water overlying the sediment (as in closed-chamber or core incubations). This model is also based on mass conservation and is referred to as the water column model (WM).

A complete model statement of lugworm bio-irrigation thus requires the combined development of a specific FM, TM and WM. Here we will investigate six model statements, which incorporate different levels of model complexity (Table 2). Two aspects determine the "complexity" of a given model: the number of model parameters (more "complex" models include more parameters) and the solution method (numerical solutions are more "complex" than analytical solutions). We start by formulating three basic models, which we refer to as the 3D, 2D and 1D baseline models. These models adopt a similar mechanistic approach, trying to capture the essential processes that determine lugworm

Table 1. List of symbols.

Symbol	Units	Meaning
R_c	L	radius of micro-environment
A_c	L^2	cross-sectional area micro-environment
H_s	L	height of sediment in micro-environment
H_w	L	height of overlying water column
n	L^{-2}	density of organisms
R_b, R_{fp}	L	burrow radius, radius of feeding pocket
A_{fp}	L^2	surface area feeding pocket
L_{gal}, L_{shaft}	L	length of lugworm burrow gallery, length of tail shaft
d	L	eccentric distance of lugworm burrow
$H_{fp} = L_{shaft}$	L	depth location of the centre of the feeding pocket
H_{iz}	L	injection depth in 1D model
R_{iz}	L	half-width injection zone in 1D model
$\mathbf{v}$, $\mathbf{v}_d$	$L\,T^{-1}$	pore water velocity, Darcy velocity
Γ	T^{-1}	injection rate
ϕ	—	sediment porosity
p, p_e	$M\,L^{-1}\,T^{-2}$	pore water pressure, excess pore water pressure
g	$L\,T^{-2}$	gravitational acceleration
ρ	$M\,L^{-3}$	density pore water
η	$M\,L^{-1}\,T^{-1}$	dynamic viscosity pore water
k	L^2	permeability
Q	$L^3\,T^{-1}$	pumping rate lugworm
C^{pw}, C^{bw}, C^{ow}	$M\,L^{-3}$	tracer concentration in pore water, burrow, overlying water
$\mathbf{D}$	$L^2\,T^{-1}$	hydrodynamic dispersion tensor
D^{mol}	$L^2\,T^{-1}$	molecular diffusion coefficient
d_{50}	L	median grain size
V^{ow}, V^s	L^3	volume of overlying water, volume of sediment
β	—	diffusion enhancement factor
κ	—	percolation area restriction factor

bio-irrigation, while making abstraction of irrelevant details. Essentially, these 3D/2D/1D baseline models have an analogous structure, but differ in the detail with which the geometry of the lugworm burrow is described. In due course, these baseline models are then compared to simplified or extended versions (Table 2). Such modifications of the baseline models can be inspired from a mechanistic point of view, but can also include ad-hoc model adjustments that simply improve the model fit to the data (see below).

b. Baseline models

Under natural conditions, the pore water flow pattern induced by *A. marina* will be clearly three-dimensional (3D). To reproduce the fine details of this 3D bio-irrigation pattern, one can implement an explicit description of the J-shaped burrow geometry and the surrounding sediment (Fig. 1a). Such a comprehensive 3D description is feasible in present-day modeling packages, and was recently explored by Meysman *et al.* (2005). This

Table 2. Overview of the different models that are used in simulations. FM = Flow Model. TM = Transport Model. WM = Water column Model. N = numerical model solution. A = analytical model solution. # Par = number of model parameters.

Model version	FM	TM	WM	# Par	Specific features
3D baseline	N	N	N	16	J-shaped burrow
2D baseline	N	N	N	13	Simple feeding pocket (spherical)
2D extended	N	N	N	14	Elongated feeding pocket (ellipsoidal)
1D baseline	A	N	N	13	Injection zone = width feeding pocket
1D simplified	A	A	A	11	Infinitely small injection zone, no hydrodynamic dispersion
1D extended	A	N	N	15	Enlarged injection zone + enhanced diffusion + feeding funnel

3D model of the lugworm burrow is the most complex description explored here (Fig. 1a). While Meysman *et al.* (2005) only examined the flow model, here we take a further step and couple the 3D FM to corresponding TM and WM. The resulting bio-irrigation model uses three spatial coordinates (x, y and z; Table 3) and is referred to the "3D baseline model" (Table 2).

Following the principle of Occam's razor, one could ask whether all this 3D detail is necessary to capture the relevant features of the lugworm's bio-irrigation. Reactive transport simulations coupled to three-dimensional flow fields are notorious consumers of computational resources. Moreover, to keep memory and runtime requirements within limits, 3D models have to use coarser discretization grids as compared to 2D and 1D counterparts (Fig. 2). Coarser grids typically enhance numerical diffusion, and may create accuracy problems when resolving the steep concentration gradients of highly reactive constituents (e.g. O_2). Accordingly, there is a clear advantage in simplifying models to a lower dimensionality in terms of computation time, storage space and numerical accuracy. In addition, simpler models contain less parameters. Consequently, it is easier to interpret their output and to perform a parameter sensitivity analysis.

Recently, Meysman *et al.* (2006) proposed a simplified 2D version of the 3D flow model by Meysman *et al.* (2005) incorporating two idealizations. (1) The burrow structure only forms a small obstacle for the pore water flow, and hence, it has a negligible effect on the flow pattern. (2) Transfer by diffusion across the burrow walls can be neglected when compared to burrow water injection via the feeding pocket. Under these two conditions, Meysman *et al.* (2006) argued that the lugworm's feeding pocket can be modeled as a spherical source of burrow water, and so the model domain acquires an axial symmetry (Fig. 2b). In other words, the geometry of the burrow itself becomes irrelevant, and the only important biological parameters are the location/shape of the feeding pocket and the pumping rate. Physically, the model domain still represents a 3D sediment zone, yet mathematically, the model now classifies as a 2D model, incorporating only two coordinates (the depth z and the distance r from the central symmetry axis). This combination of

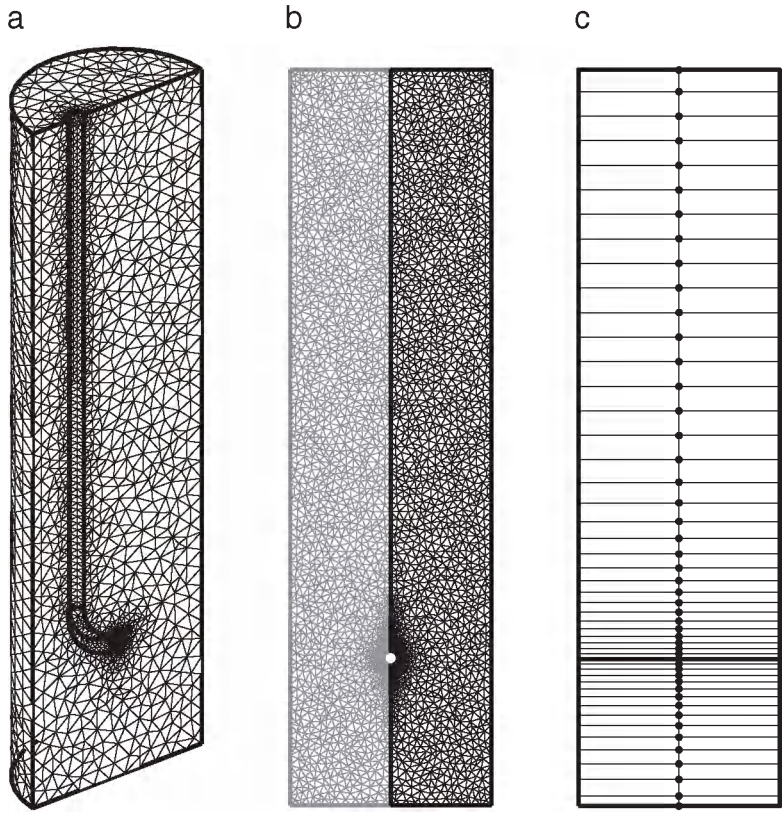

Figure 2. Finite element meshes used to discretize the sediment domain. (a) 3D model—actual grid. (b) 2D axi-symmetric model—actual grid. (c) 1D model—conceptual sketch of discretization (the grid used was much finer).

an axisymmetric FM with a corresponding TM and WM is further referred to as the "2D baseline model" (Table 2).

In the past, the advective bio-irrigation resulting from burrow water injection has been described via 1D formulations (Benoit *et al.*, 1991; Timmermann *et al.*, 2002, 2003). In a third step, we can further reduce the geometrical complexity to arrive at a similar 1D description. The common feature of these 1D models is that they have no explicit representation of the burrow, and so burrow water does not pass through a particular "boundary surface" like that of the injection pocket. Instead, these models assume that burrow water is homogeneously injected within a specific depth layer, and subsequently, percolates upwards through a sediment column with a constant cross-sectional area (Fig. 1c). Sometimes the injection zone is infinitely thin, thus resulting in a so-called point-injection model (Benoit *et al.*, 1991). Other models consider a finite injection zone with a uniform injection rate per unit of depth (Timmermann *et al.*, 2002, 2003). The baseline 1D model presented here

(Table 2) is obtained by properly averaging the 2D baseline model (detailed below), and so, the injection layer is of the same thickness as the feeding pocket. Again, the model domain remains physically 3D, but the description is mathematically 1D (only the depth z is used as a spatial coordinate).

c. Model domain

The modeled sediment domain is exactly the same in the baseline 3D/2D/1D models, but for the internal details of the burrow geometry (Fig. 1). This so-called "Arenicola domain" comprises a cylindrical volume of radius R_c, containing a sediment column of depth H_s and an overlying water column of height H_w. It represents either a territory under natural conditions, or the cylindrical container/aquarium in which lab incubations are carried out. Each domain contains a single lugworm, and so, the radius is calculated from $R_c = 1/\sqrt{\pi n}$, where n denotes the lugworm density [organisms per unit area]. For simplicity, the sediment-water interface is considered a flat surface, neglecting any micro-topography created by the lugworm's feeding pit and defecation mound.

The difference between 3D/2D/1D baseline models essentially concerns the representation of the burrow. In the 3D baseline model, the J-shaped burrow has a curved cylindrical form, which is described analytically using standard geometrical shape functions in FEMLAB (Fig. 2a, see also Meysman *et al.*, 2005 for details). The J-shaped burrow is placed along the middle plane of the domain, with the centre of the feeding pocket at a distance d from the central axis (Fig. 1a). This way, the geometry of the lugworm burrow depends on five parameters: (1) the burrow radius R_b, (2) the length of the gallery L_{gal}, (3) the length of the tail shaft L_{shaft}, (4) the radius of the spherical feeding pocket R_{fp}, and (5) the eccentric distance d. The feeding pocket is located at the same depth as the horizontal gallery, i.e., $H_{fp} \equiv L_{shaft}$. Because the burrow is placed in the middle plane, the lugworm domain becomes symmetric, and so, only half of the 3D domain has to be effectively discretized (Fig. 2a). In the 2D baseline model (Fig. 1b) the burrow shaft is omitted, solely retaining the spherical void of the feeding pocket, which is positioned along the symmetry axis of the cylindrical sediment core. This idealization significantly reduces the model complexity. Instead of five, the burrow geometry is now described by two parameters: (1) the feeding pocket depth H_{fp}, and (2) the feeding pocket radius R_{fp}. In the 1D baseline model, all geometrical features of the burrow are completely abandoned. The injection of burrow water now occurs homogeneously within a sediment layer that has the same thickness as the feeding pocket (Fig. 1c). This injection zone is centered at depth $H_{iz} \equiv H_{fp}$, and its half-width equals the radius of the feeding pocket $R_{iz} \equiv R_{fp}$. This way, it is clear that the baseline 1D model also depends on two "burrow" parameters. In other words, the baseline 1D model exhibits the same degree of complexity as the 2D baseline model with respect to the number of parameters (Table 2).

A non-trivial assumption underlying all models presented here is the homogeneity of the model domain. Homogeneity implies that properties (porosity, permeability etc.) have uniform values throughout the sediment domain. Under natural conditions, sediment

Table 3. Overview of the operators used in Cartesian and cylindrical coordinates. In 3D models, Cartesian coordinates (x, y, z) are used and the full form of the operators is implemented. 2D models use cylindrical coordinates (r, z), and due to the axial symmetry, the terms containing derivatives with respect to the angular coordinate θ are dropped. 1D models are specified in terms of the Cartesian coordinate z, and so all terms containing the derivatives with respect to x and y vanish. Additional details on the above coordinate systems and operators can be found in Bronshtein *et al.* (2003).

Coordinate system	Cartesian	Cylindrical
Coordinates/unit vectors	$x, y, z/\mathbf{e}_x, \mathbf{e}_y, \mathbf{e}_z$	$r, \theta, z/\mathbf{e}_r, \mathbf{e}_\theta, \mathbf{e}_z$
∇ operator	$\mathbf{e}_x \frac{\partial}{\partial x} + \mathbf{e}_y \frac{\partial}{\partial y} + \mathbf{e}_z \frac{\partial}{\partial z}$	$\mathbf{e}_r \frac{\partial}{\partial r} + \mathbf{e}_\theta \frac{1}{r}\frac{\partial}{\partial \theta} + \mathbf{e}_z \frac{\partial}{\partial z}$
∇p (gradient of scalar)	$\mathbf{e}_x \frac{\partial p}{\partial x} + \mathbf{e}_y \frac{\partial p}{\partial y} + \mathbf{e}_z \frac{\partial p}{\partial z}$	$\mathbf{e}_r \frac{\partial p}{\partial r} + \mathbf{e}_\theta \frac{1}{r}\frac{\partial p}{\partial \theta} + \mathbf{e}_z \frac{\partial p}{\partial z}$
$\nabla \cdot \mathbf{v}$ (divergence of vector)	$\frac{\partial v_x}{\partial x} + \frac{\partial v_y}{\partial y} + \frac{\partial v_z}{\partial z}$	$\frac{1}{r}\frac{\partial}{\partial r}(r v_r) + \frac{1}{r}\frac{\partial v_\theta}{\partial \theta} + \frac{\partial v_z}{\partial z}$
$\nabla^2 p_e$ (Laplacian of scalar)	$\frac{\partial^2 p_e}{\partial x^2} + \frac{\partial^2 p_e}{\partial y^2} + \frac{\partial^2 p_e}{\partial z^2}$	$\frac{1}{r}\frac{\partial}{\partial r}\left(r\frac{\partial p_e}{\partial r}\right) + \frac{1}{r^2}\frac{\partial^2 p_e}{\partial \theta^2} + \frac{\partial^2 p_e}{\partial z^2}$

reworking by *A. marina* is thought to lead to considerable spatial heterogeneity in sediment properties (Meadows and Tait, 1989; Jones and Jago, 1993). A coarse sediment layer is often observed at the level of the gallery and feeding pocket, attributed due to selective particle ingestion. Equally, the zone below the feeding funnel, where sediment slopes downwards to the feeding pocket, is considered to have distinct properties in comparison to the surrounding sediment. Still, in the models presented here, we do not include such spatial zonation in porosity and permeability because of three reasons. Firstly, implementing the principle of Occam's razor, we need to explore the most parsimonious model formulation first. So, we investigate to what extent the assumption of homogeneity can explain the existing observations. Secondly, past discussions on heterogeneity within lugworm habitat have been rather qualitative. Quantitative data on the extent of the permeable shell layer and the feeding funnel are lacking, nor are data available on the actual porosity and permeability values within these zones. Thirdly, spatial heterogeneity requires time to develop. The laboratory incubations used here for model validation, start from an initially homogeneous sediment, involve only short acclimation periods, and have limited incubation periods (1 hr–1 day). We assume that this time span is too short to develop significant heterogeneity.

d. Flow model (momentum conservation)

Irrespective of the dimensionality of the model, the flow pattern in the pore water is governed by the continuity equation for an incompressible fluid (Freeze and Cherry, 1979; Bear and Bachmat, 1991)

$$\nabla \cdot (\phi \mathbf{v}) = \Gamma \tag{1}$$

where $\mathbf{v}$ is the pore water velocity and ϕ the porosity. The source term Γ represents the injection of burrow water per unit of volume. Note that the operator ∇ in Cartesian coordinates, as used in the 3D and 1D models, differs from that in cylindrical coordinates as used in the 2D models (see Table 3). The continuity equation (1) is the common starting point for the 1D/2D/3D baseline models. The subsequent procedure, however, differs between 1D (no representation of the burrow) and 2D/3D (explicit representation of burrow). In the 1D model, the lugworm's injection of burrow water into the sediment is emulated as an "internal" source. Technically, one imposes a certain source function $\Gamma \neq 0$ upon the model, and subsequently, the velocity field is directly calculated from Eq. (1). In contrast, in the 2D and 3D model, the injected burrow water enters the model via an "external" source, i.e., implemented via the boundary condition along the feeding pocket. As a result, the physically *ad hoc* source term Γ is no longer required in 2D/3D.

Instead, the flow model formulation is now closed by the substitution of Darcy's law as a constitutive equation in the continuity equation (1). The resulting equation set can be presented in the same form for 3D and 2D (see Meysman *et al.* (2005) for 3D, and Meysman *et al.* (2006) for the 2D case). Darcy's Law can be stated in the general form as (Freeze and Cherry, 1979; Bear and Bachmat, 1991)

$$\mathbf{v} = -\frac{k}{\phi \eta}(\nabla p - \rho g \nabla z) \tag{2}$$

where k denotes the permeability of the sediment, η the fluid viscosity, ρ the density of the pore water, p the pressure, g is the gravitational constant, and z represents the depth coordinate measured downwards from the sediment water interface (SWI). Assuming that (1) porosity and permeability remain constant over the sediment domain and (2) the pore water is incompressible, isothermal and of uniform salinity, the substitution of Darcy's Law (2) into the continuity equation (1) eventually leads to the Laplace equation (Meysman *et al.*, 2005)

$$\nabla^2 p_e = 0 \tag{3}$$

where $p_e \equiv p - (p_{SWI} + \rho g z)$ is the pressure in excess over the hydrostatic pressure, and p_{SWI} is the constant pressure at the SWI. The Laplace equation (3) produces the excess pressure distribution in the pore water, from which one can subsequently calculate the associated velocity vector field by means of Eq. (2).

The solution of the Laplace equation (3) requires appropriate boundary conditions both externally, along the outer boundaries of the sediment domain, and internally, along the surface of the J-shaped burrow (3D) and/or the feeding pocket (3D/2D). The formulation of the external boundary conditions is identical in 3D and 2D models. At the SWI, we adopt a constant pressure p_{SWI}, so the pore water freely flows out of the sediment and all flowlines are normal to the SWI. At the lower and lateral boundaries, we impose the no-flux

condition $\mathbf{v} \cdot \mathbf{n} \equiv 0$. Under laboratory conditions, the sediment is sealed off by the core lining, while under natural conditions, we assume a full coverage of the tidal flat by adjacent lugworm domains and that the flow does not penetrate deeper layers.

The conditions specified at the internal boundaries require more consideration. Both in the 2D and 3D model set-up, the feeding pocket forms the actual location where the lugworm pumps the burrow water into the sediment. As discussed in Meysman *et al.* (2005), transient pumping activity should not significantly affect the flow pattern, and so the lugworm can be modelled as a mechanical pump with a steady pumping rate Q. The total water flow Q pumped by the lugworm should leave the feeding pocket through the surface S_{fp}

$$Q = \oint_{S_{fp}} [\phi \mathbf{v}] d\mathbf{S} \tag{4}$$

When pumping, the lugworm exerts a constant excess pressure $p_e \equiv p_{fp}$ along the surface of the feeding pocket. However, parameter values for p_{fp} are not available in the literature, and typically, the lugworm's pumping rate Q is reported. In the flow simulations, we used the lugworm's pumping rate Q as an input parameter, while still imposing an isobaric pressure $p_e \equiv p_{fp}$ along the surface of the feeding pocket. Taking advantage of the linearity of the problem, each flow simulation was preceded by a test simulation to determine the unknown value of p_{fp} so that the integral (4) matches the specified input value for Q. In the 3D model, additional boundary conditions should be specified along the burrow wall. We will assume that burrow walls are impermeable to flow, and hence the $\mathbf{v} \cdot \mathbf{n} \equiv 0$ condition holds. This assumption will be justified *a posteriori* (see discussion below).

The 2D and 3D baseline FM are completely described by the equation set (2)–(4). As noted before, the 1D baseline FM is not derived as the solution of a separate model, but represents the laterally average of the velocity field obtained from the 2D model, i.e.,

$$v^{1D}(z) = \langle \mathbf{v}^{2D} \rangle = \frac{1}{\pi \{R_c\}^2} \int_0^{R_c} v_z^{2D}(z, r) 2\pi r dr. \tag{5}$$

Since the 2D model generates a radial symmetric velocity field, all radial components of the 2D velocity vector vanish upon averaging, and hence, the velocity vector only retains a vertical component (5) pointing upwards (opposite to the direction of the z-axis). Although theoretically appealing, Eq. (5) is of little practical use: it cannot be used without first calculating the 2D model solution. However, there is an alternative to directly calculate $v^{1D}(z)$, i.e., by calculating the depth dependent discharge $\Gamma(z)$ within the injection zone enveloping the feeding pocket. When we assume that burrow water is discharged homogeneously across the surface of the spherical feeding pocket, this discharge actually

becomes constant throughout the injection interval (horizontal slices of equal thickness through a sphere have an equal surface area; Bronshtein *et al.*, 2003)

$$\Gamma(z) = \frac{1}{2R_{iz}} \frac{Q}{\phi A_c} \quad \text{for} \quad (H_{iz} - R_{iz}) \le z \le (H_{iz} + R_{iz}) \tag{6}$$

where A_c is the surface area of the core. For an incompressible fluid, and a sediment configuration only permitting upward flow, the flow velocity at certain horizon should scale to the total fluid input below that horizon. Accordingly, the 1D velocity pattern that results from (6) is

$$\begin{cases} 0 \le z \le (H_{iz} - R_{iz}): & v(z) = -Q/[\phi A_c] \\ (H_{iz} - R_{iz}) \le z \le (H_{iz} + R_{iz}): & v(z) = -\frac{1}{2}(1 + H_{iz}/R_{iz} - z/R_{iz})Q/[\phi A_c] \\ (H_{iz} + R_{iz}) \le z \le H_s: & v(z) = 0 \end{cases} \tag{7}$$

Accordingly, one obtains three distinct zones in the 1D flow field. Below the injection zone, the advective velocity vanishes. Within injection zone, the advective velocity linearly increases from zero to the value $Q/[\phi A_c]$. Above the injection zone, the advective velocity remains constant (see also Fig. 3b in Meysman *et al.*, 2006).

e. Transport model (mass conservation)

Once the velocity field **v** is computed from the flow model, this quantity can be implemented in the mass conservation equation for a pore water constituent. Here, we specifically consider the solutes Br^- and NO_3^-, which are used as inert tracers in the validation experiments. For 1D/2D/3D baseline models, the applicable transport equation for a conservative tracer can be cast in the same generic form (Bear and Bachmat, 1991; Boudreau, 1997; Meysman *et al.*, 2006)

$$\frac{\partial C^{pw}}{\partial t} + \nabla \cdot (-\mathbf{D} \cdot \nabla C^{pw} + \mathbf{v} C^{pw}) - \Gamma C^{bw} = 0 \tag{8}$$

where **D** denotes the hydrodynamic dispersion tensor (see Table 3 for a proper definition of the operators in (8)). Note that superscripts are used to distinguish different tracer concentrations, i.e. the pore water concentration C^{pw}, the burrow water concentration C^{bw}, and the concentration in the overlying water column C^{ow} (which is used below). As noted above, the distributed source term Γ only appears in the 1D model equation. Because the porosity is assumed constant over the sediment domain, porosity terms do not appear in equation (8). The hydrodynamic dispersion tensor **D** includes the effects of both molecular diffusion and mechanical dispersion, and is typically decomposed as $\mathbf{D} = \mathbf{D}^{mol} + \mathbf{D}^{mech}$ (Bear and Bachmat, 1991). The tensor due molecular diffusion can be stated as

$$\mathbf{D}^{mol} = [1 - 2 \ln \phi]^{-1} D^{mol} \mathbf{I} \tag{9}$$

where $\mathbf{I}$ denotes the unit tensor, D^{mol} represents the scalar molecular diffusion coefficient, and the factor $[1 - 2 \ln \phi]^{-1}$ represents a correction for tortuosity (Boudreau, 1996b). The molecular diffusion coefficient D^{mol} for Br^- and NO_3^- are calculated as a function of temperature T and salinity S using the relations given in Boudreau (1997). The mechanical dispersion tensor $\mathbf{D}^{mech}$ is typically expressed as (Freeze and Cherry, 1979; Lichtner, 1996)

$$\mathbf{D}^{mech} = D_T \mathbf{I} + \frac{1}{\|\mathbf{v}\|^2} (D_L - D_T) \mathbf{v}\mathbf{v}^T \tag{10}$$

where D_T and D_L are the transversal and longitudinal dispersion coefficients. The constitutive expression for the latter coefficients are taken from Oelkers (1996)

$$D_T = D^{mol} 0.5 \{Pe\}^{1.2} \tag{11}$$

$$D_L = D^{mol} 0.015 \{Pe\}^{1.1} \tag{12}$$

which are valid for Péclet numbers in the range 1–100. The dimensionless Péclet number is calculated as $Pe \equiv d_{50} \|\mathbf{v}\| / D^{mol}$, where d_{50} denotes the median grain size.

Eq. (8) produces the tracer concentration field over the lugworm domain, given a proper set of initial and boundary conditions. As initial condition, we assume a uniform tracer concentration C_0^{pw} in the pore water. At the sediment-water interface, we assume that advective transport dominates diffusion, and hence, the convective flux condition $\mathbf{n} \cdot (D \nabla C^{pw}) \equiv 0$ is implemented. At the lower and lateral side of the domain, the boundary is impenetrable to mass, i.e., $\mathbf{n} \cdot (-D \nabla C^{pw} + C^{pw} \mathbf{v}) \equiv 0$. In the 3D baseline TM, the same no-flux condition is specified at the burrow wall. Furthermore, we assume that the burrow is a fully mixed volume, and that the tracer concentration in the burrow water is not influenced by the lugworm's metabolism, i.e., $C^{bw}(t) = C^{ow}(t)$. Consequently, the water injected across the surface of the feeding pocket has the same composition as that in the overlying water column. Accordingly, in 2D and 3D models, the water that leaves the feeding pocket has the concentration $C^{ow}(t)$. In the 1D model, the injection of burrow water is described by the source term in Eq. (8), where Γ is given by Eq. (6), and $C^{bw} = C^{ow}(t)$. The time-dependent value of $C^{ow}(t)$ is obtained from the model of the overlying water column, as described in the next section.

f. Water column model

The water column overlying the sediment is assumed to be well mixed, and the initial tracer concentration is denoted C_0^{ow}. Accordingly, for a passive tracer, the total inventory in the lugworm domain should remain constant, i.e.,

$$V^{ow} C^{ow}(t) + \int_{V^s} \phi C^{pw}(t) dV^s = V^{ow} C_0^{ow} + \int_{V^s} \phi C_0^{pw} dV^s \tag{13}$$

where V^s is the volume of the sediment and V^{ow} stands for the volume of the overlying water. Hereby, we ignore the small volume of water stored in the burrow. Expression (13) can be re-arranged to obtain following explicit expression for the tracer concentration in the overlying water column:

$$C^{ow}(t) = C_0^{ow} + \frac{\phi}{V^{ow}} \int_{V^s} (C_0^{pw} - C^{pw}(t)) dV^s. \tag{14}$$

The integral on the right hand side can be numerically evaluated by standard integration procedures.

g. Simplified and extended model versions

The 1D/2D/3D baseline models differ only in the way the lugworm's burrow geometry is described. In a first step, we will investigate how these three baseline models reproduce the data from the inert tracer experiments. When comparing model output and data, it will prove useful to adapt these baseline descriptions, and in due course, we will investigate three such "modified models" (Table 2). A first modified model involves a further simplification of the 1D baseline model. Rather than scaling the injection zone to the finite diameter of the feeding pocket, we explore the asymptotic case where the injection zone has a negligible width. Mathematically, this means that we take the limit of Eq. (7) for $R_{iz} \rightarrow 0$. This so-called "point injection model" splits the sediment domain into two zones, above and below the injection depth. At the internal boundary, the lugworm's discharge of burrow water now causes a jump discontinuity in the pore water velocity. In terms of parameters, the reduction in model complexity is quite moderate. The "simplified 1D model" incorporates one parameter less than its baseline counterpart. However, in terms of model solution, the reduction in model complexity is quite substantial. The coupling of the simplified TM to the associated WM allows an analytical solution to Eq. (14) when hydrodynamic dispersion is ignored. The full details of this solution procedure are given in the Appendix.

A second modified model involves the extension of the 2D baseline model with a more complex geometry. We replace the default spherical feeding pocket by an elliptic one with the long axis in parallel to the vertical. In terms of model complexity, this "extended 2D model" requires the introduction of one additional parameter. Instead of one radius R_{fp}, the elliptic feeding pocket is now described by a minor radius $R_{fp}^{\min}$ (horizontally) and a major radius $R_{fp}^{\max}$ (vertically). This modification of the feeding pocket can be justified for several reasons. Under natural conditions, it is sometimes observed that the gallery is curved upwards, creating such a vertical extension of the injection zone. Also, the lugworm may reposition during incubation. As a result, the injection depth may shift over the course of incubation so that burrow water is injected over a larger horizon. In a steady state simulation, this dynamic phenomenon can be emulated by an apparent extension of the injection zone.

Finally, a third modified model is referred to as the "extended 1D model," and is specifically developed to allow comparison with the 1D model of lugworm bio-irrigation proposed by Timmermann *et al.* (2002, 2003). This model requires two separate extensions of our baseline 1D model. Firstly, in the model by Timmermann *et al.* (2002), the diffusion coefficient $D^{eff} = [1 - 2 \ln \phi]^{-1} D^{mol}$ is multiplied by a diffusion enhancement factor β, which is introduced to account for "pore water mixing due to meiofauna and dispersion due to hydrodynamical flows" (Timmermann *et al.*, 2002). No *a priori* information is available on the value of this β factor, and hence, Timmermann *et al.* (2002) used it as an adjustable factor to improve model fits. Secondly, the model by Timmermann *et al.* (2002) distinguishes two concentric zones within the sediment. It is assumed that only a central "percolation zone" of radius R_{pz} is truly affected by lugworm bio-irrigation, while an outer "stagnant zone" is not influenced. The percolation zone has a cross-sectional area $A_{pz} = \pi R_{pz}^2$, and we denote the (radially averaged) pore water concentration within this zone as $C^{pw-pz}(z, t)$. Similarly, the stagnant zone is of area $A_{sz} = \pi(R_c^2 - R_{pz}^2)$, and has the radially-averaged pore water concentration $C^{pw-sz}(z, t)$. The interpretation by Timmermann *et al.* (2002) is that this percolation zone coincides—in cross-section at least—with the lugworm's feeding funnel through which water is transported backward to the surface. To this end, the scaling factor $\kappa = A_{pz}/(A_{pz} + A_{sz})$ is introduced, which varies between 0 and 1. Small values ($\kappa \to 0$) indicate selective percolation through a small feeding funnel. In contrast, large values ($\kappa \to 1$) indicate the absence of a feeding funnel, so that the injected water percolates homogeneously upwards across the whole section of the sediment domain. Based on mass conservation, it is readily clear that the advective velocity $v^{pz}(z)$ and the source term $\Gamma^{pz}(z)$ within the percolation zone are given by expressions (7) and (6) respectively, where the full core area A_c now needs to be replaced by the percolation area A_{pz}. This way, one obtains that $v^{pz}(z) = \kappa^{-1} v(z)$ and $\Gamma^{pz}(z) = \kappa^{-1}\Gamma(z)$. Note that the percolation zone in the model cannot be equated with the feeding funnel as such, because the percolation zone extends beyond the feeding depth all the way down to the bottom of the core. The governing equation within the percolation zone becomes a modified version of the mass balance (8) (Timmermann *et al.*, 2002)

$$\frac{\partial C^{pw-pz}}{\partial t} = \beta D^{eff} \frac{\partial^2 C^{pw-pz}}{\partial z^2} + \kappa^{-1} \frac{\partial [v(z) C^{pw-pz}]}{\partial z} - \kappa^{-1} \Gamma(z) C^{bw}(t) \tag{15}$$

where β is the diffusion enhancement factor and κ is the percolation factor. The solution of equation (15) provides the depth profiles $C^{pw-pz}(z)$ in the percolation zone. The experimental data profile however contains the pore water concentration averaged over the whole width of the sediment domain. Properly averaging the concentrations within the separate zones thus leads to

$$C^{pw}(z, t) = \kappa C^{pw-pz}(z, t) + (1 - \kappa) C^{pw-sz}(z, t) \tag{16}$$

where $C^{pw-sz}(z, t)$ is simply equated to the background concentration of the tracer in the pore water.

In summary, the extended 1D model by Timmermann *et al.* (2002) introduces two new fitting coefficients: the restriction factor κ and the diffusion enhancement factor β. In total, the extended 1D model thus incorporates 15 parameters, only 1 parameter less than the 3D baseline model. When $\kappa \equiv \beta \equiv 1$, the extended 1D model simplifies to the baseline 1D version.

h. Numerical issues

The Laplace equation (3) for 3D/2D models, and the reactive transport equation (8) for 3D/2D/1D models are solved numerically using the finite element package FEMLAB™ version 3.0a (www.comsol.com). The WM equation (14) is coupled to the TM via so-called *integration coupling variable* approach. As noted before, the velocity field in the 1D case is analytically solved for. Figure 2 shows the grids over the sediment domain employed in the different models. Triangular and tetrahedrical unstructured finite element meshes are used in 2D and 3D simulations respectively. In the 3D case, the mesh is refined near the burrow wall and the feeding pocket, since the largest pressure and concentration gradients occur in this zone. Similarly, in the 2D and 1D case, a finer mesh is used in the zone of the feeding pocket. For presentation purposes, Figure 2c provides only a sketch of the grid used in the 1D case. The actual mesh adopts a much finer spatial resolution.

In the 1D and 2D simulations, the hydromechanical dispersion implemented in the model proved sufficient to ensure the numeric stability of the computational approach. However, in 3D simulations, coarser meshes were used. As a result, the level of hydromechanical dispersion in the model sometimes proved insufficient to ensure a stable integration procedure. In these cases, the artificial stabilization option termed "anisotropic diffusion" in FEMLAB™ was turned on. This technical measure did however not influence the simulated concentrations profiles. Advection is the dominant transport process shaping the tracer distributions, and dispersion only plays a minor role. Accordingly, the slight increase in the effective dispersion coefficient due to artificial stabilization did not affect the profiles.

i. Inert tracer experiments

In the previous sections we have presented 3 baseline models and 3 modified versions of these baseline models. To validate these six models, the simulation output was compared with results from two distinct types of conservative tracer experiments, referred to as "injection" and "flushing" incubations. Both types of incubations have the same basic set-up, i.e., a sediment core with a fixed volume of overlying water to which a single lugworm is added (Fig. 3). In the "injection" experiment, the inert tracer is added to the overlying water column and its appearance in the pore water is measured after a certain incubation period (Fig. 3a). In the "flushing" experiment, the pore water is initially preloaded with a high concentration of the inert tracer, and the subsequent emergence of the tracer in the overlying water is monitored (Fig. 3b). For both injection and flushing

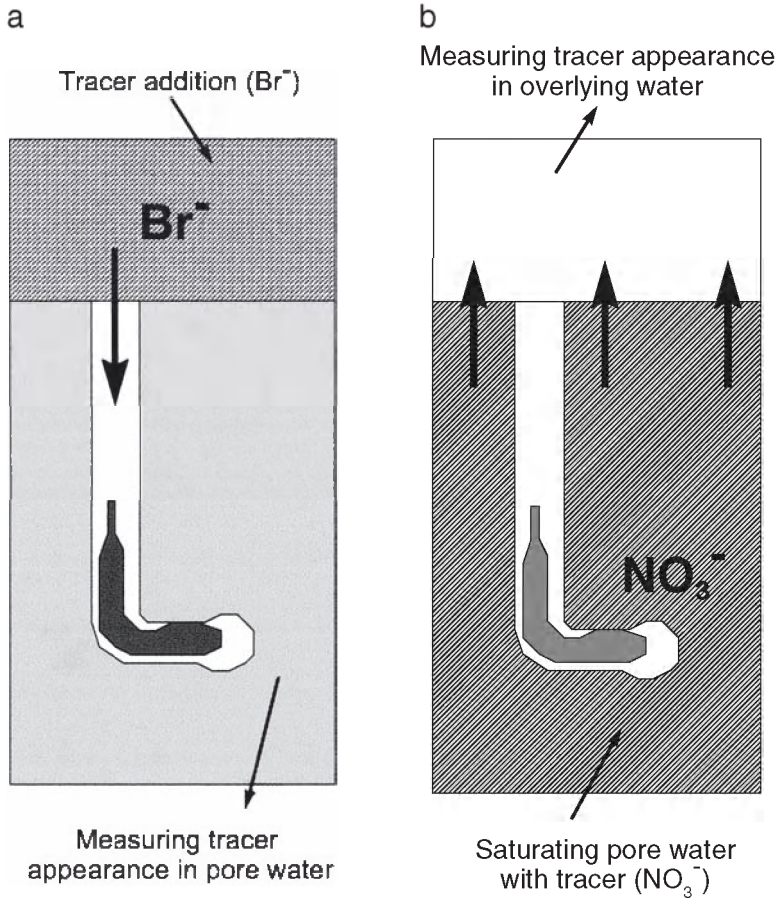

Figure 3. Schematic representation of the inert tracer experiments: (a) injection experiment—tracer is initially added to the overlying water and its distribution in the sediment analyzed afterwards; (b) flushing experiment—sediment is pre-loaded with tracer-rich pore water and the appearance of tracer is monitored in the (initially tracer-free) overlying water.

experiments, the available data and the constraining of model parameters are discussed in detail in Meysman *et al.* (2006). Only a short overview of the dataset is given here.

The "injection" data set is based on the Br^- incubations conducted by Rasmussen *et al.* (1998). In six cores, the overlying water was spiked with Br^-, and after a short incubation period of ~1–2 hr, the depth profile of Br^- was determined through core slicing and pore water extraction. The lugworm's depth location was measured at the end of experiment. Details on experimental set-up, core sectioning and analytical methods can be found in Rasmussen *et al.* (1998), while a more extensive description of the dataset and experimental parameters is given in Timmermann *et al.* (2002). To mimic the Br^- accumulation at

depth observed in the core incubations, we performed dynamical simulations using the 3D/2D/1D models over the exact time interval of the experimental incubation. The output of these simulations consists respectively of 3D/2D/1D dimensional distributions of the Br^- concentration in the pore water. To allow comparison with the 1D data profiles, the model output from 3D and 2D models was laterally integrated to produce the average Br^- concentration within a given depth layer.

The data set of the flushing experiment has been reported in Meysman *et al.* (2006). Two sediment cores were initially pre-loaded with a high concentration of NO_3^- in pore water. Then the overlying water was carefully removed and replaced by tracer-free sea water and one lugworm was introduced to each core. The appearance of the nitrate in the well-mixed and aerated overlying water was monitored on-line with a nitrate electrode (Unisense NOx biosensor). Incubations were carried out with clean sand and filtered seawater, and the time span of experiment was short, so that nitrate could be used as a conservative tracer (Meysman *et al.*, 2006).

3. Simulation results

a. Flowline patterns

Figure 4 shows the flowline pattern simulated by the three baseline models. The parameter set used in these simulations is summarized in Tables 4 and 5. The flowline patterns in 3D case (Fig. 4a) and 2D case (Fig. 4b) exhibit a strong similarity, and the velocity field can roughly be separated into two distinct zones. In a first "irradiation" zone, the flowlines originate from the feeding pocket and propagate uniformly in all directions, including downwards from the feeding pocket. Eventually all flowlines curve upwards to the sediment-water interface and align in parallel to the vertical. The latter zone is termed the "percolation" zone. The influence of the J-shaped burrow in the 3D model appears to be moderate (Fig. 4a). This is not unsurprising. Since a no-flux boundary condition is applied along the burrow walls, the burrow essentially acts as an impenetrable object with respect to the pore water flow. For a typical lugworm density and a typical burrow size, the volume of the burrow takes up only around 0.1% of the volume of the surrounding sediment (Meysman *et al.*, 2006). Accordingly, the size of the impenetrable obstacle is small, and therefore, the burrow in 3D only introduces a slight distortion of the axial symmetric pattern in the corresponding 2D velocity field.

In the 1D case (Fig. 4c), the velocity field is not computed numerically, but specified directly via the analytical solution (7). This flow pattern in the 1D case differs significantly from the 2D and 3D situation. The "irradiation" zone is completely absent in 1D and only the "percolation zone" remains. All flow lines originate from the narrow feeding pocket layer where burrow water is homogeneously injected. No flow occurs beneath the feeding pocket zone (i.e. $|v_z| = 0$). Above the feeding pocket, the velocity is immediately constant and all flowlines directly align in parallel (i.e. $|v_z| = Q/[\phi A_c]$). As a result, the percolation

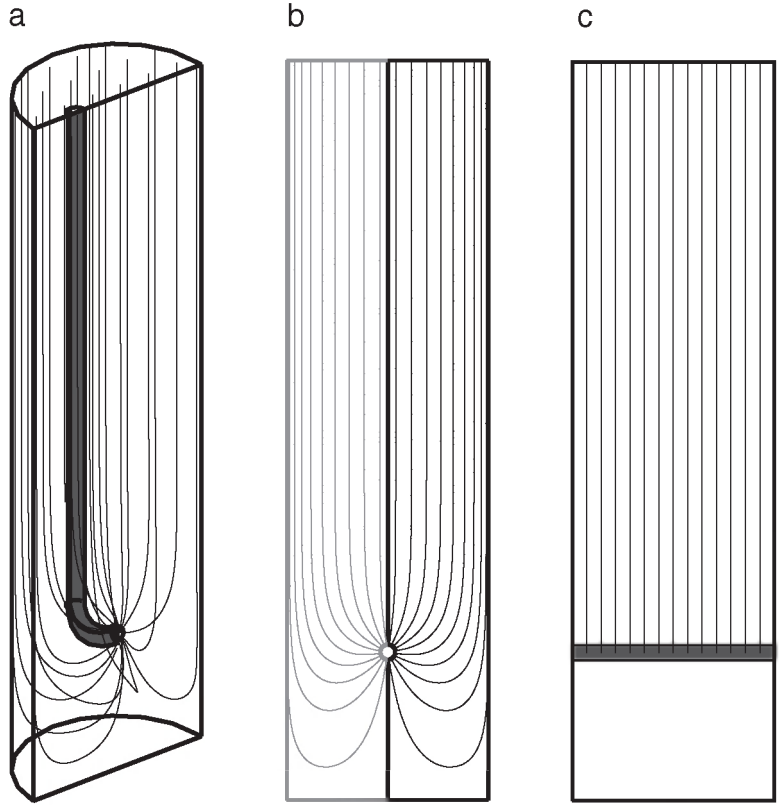

Figure 4. Flowline patterns resulting from baseline simulations: (a) 3D finite element model; (b) 2D axi-symmetric finite element model; the left part of the image was produced by mirroring the right part, which was actually computed; (c) 1D model (sketch).

zone in 1D is considerably larger than in the 2D/3D case, and now reaches down the depth of the feeding pocket. In contrast, our 2D/3D flowline simulations predict that both zones are of the same extent (Fig. 4a,b).

As our prime interest was to confront model with experiments, we only report simulations with the core diameters and feeding pocket depths that were actually used in the experiments. For sufficiently large cores (radius >5 cm), the flow pattern becomes independent of the width of the sediment domain (results not shown). For smaller cores (radius <5 cm), the flow increasingly starts to "feel" the lateral boundaries. A similar result holds for the distance between the feeding pocket and the centre of the core (significant distortion begins at approx. 5 cm). Obviously, this is an important point of attention for incubation experiments with large organisms as lugworms, since the height and diameter of the sediment domain set-up may strongly influence the obtained results.

Table 4. Parameters characterizing the experimental conditions in the "injection" experiments. Parameters values are the same for all six incubation experiments. All parameters values except for d_{50} are based on measurements as reported in Rasmussen *et al.* (1998) and Timmermann *et al.* (2002). [*] Only a qualitative indication for sediment composition was reported, i.e. the sediment was characterized as "very permeable" (Timmermann *et al.*, 2002). Based on this statement, we adopted a median grain size d_{50} = 300 μm, typifying a coarse sand flat.

Core set-up			
Core radius	R_c	cm	4.1
Sediment height	H_s	cm	30
Height overlying water column	H_w	cm	4.7
Experimental conditions			
Temperature	T	°C	15
Salinity	S	—	15
Porosity	ϕ	—	0.30
Median grain size [*]	d_{50}	μm	300

b. Injection simulations

The "injection" dataset contains six depth profiles of Br^- concentration, derived from six separate core incubations each containing a single lugworm (Rasmussen *et al.*, 1998; the letter code a–f in Figures 5–6 corresponds to their designation in Timmermann *et al.*, 2002). In a first step, we compare the 3D baseline model to the 2D baseline model, and investigate to what extent these models reproduce the profiles of the injection dataset. In a second step, we explore whether a further simplification of the 2D baseline model to the 1D baseline model is feasible. In a third step, we investigate whether and how modifications of the baseline models could improve the fit to the data.

The complete statement of the baseline models (i.e. FM + TM + WM) requires the specification of 13 parameters that are common to 1D/2D/3D models (i.e. "generic 1D/2D/3D parameters"—Tables 4 and 5). Seven of these baseline parameters adopt a common value in all six incubations (Table 4). These are the core set-up (core radius, sediment height, height overlying water), ambient conditions (salinity, temperature) and sediment properties (porosity, median grain size). Six parameters need a specific value for each incubation: the incubation time, the initial tracer concentrations in pore water and overlying water, the depth and radius of the feeding pocket, and the lugworm's pumping rate (Table 5). Both 1D and 2D baseline models include the same parameter set, and are fully determined by the specification of the above 13 parameters. Because of the more elaborate burrow geometry, the 3D baseline model requires three more parameters ("specific 3D parameters"—Table 5). A valuable facet of the injection dataset collected by Rasmussen *et al.* (1998) and Timmermann *et al.* (2002) is its completeness. Effectively, the values for all 13 generic baseline parameters could be (directly or indirectly) constrained on the basis of measurements—this procedure is extensively discussed in Meysman *et al.* (2006). For the specific 3D parameters, only the burrow radius was measured during the experiments. The other two burrow parameters, i.e. the gallery length L_{gal} and the

Table 5. Summary of parameters used in the model simulations of the "injection" experiments. [1] Parameter values constrained by direct measurements as reported in Rasmussen *et al.* (1998) and Timmermann *et al.* (2002). [2] The initial bromide concentration in the pore water C_0^s was estimated using the concentration of 0.825 mM in seawater of 33 salinity, and linearly rescaling this value to the value of 15 salinity in the experiments. [3] The radius of the feeding pocket is taken equal to the measured burrow radius. [4] The pumping rate Q is calculated from the inventory changes of the tracer in both the overlying water and the pore water using the procedure detailed in Meysman *et al.* (2006). [5] The burrow geometry in 3D is chosen in such a way that the feeding pocket has exactly the same location as in 2D, and that the burrow shaft remains at a sufficient distance from the core wall to avoid boundary effects. [6] Parameter values constrained by visual fitting of model profiles to the data.

				a	b	c	d	e	f
Common 1D/2D/3D parameters (baseline model)									
Incubation time	[1]	t_{final}	min	72	78	75.6	84	96	114
Initial concentration overlying water	[1]	C_0^{ow}	mM	12.7	10.7	13.3	10.4	13.1	12.6
Initial concentration pore water	[2]	C_0^{pw}	mM	0.3	0.3	0.3	0.3	0.3	0.3
Depth feeding pocket	[1]	H_{fp}	cm	16.0	15.0	17.0	16.0	24.0	18.0
Radius feeding pocket	[3]	R_{fp}	cm	0.15	0.25	0.30	0.25	0.30	0.35
Pumping rate	[4]	Q	$cm^3\ min^{-1}$	0.175	0.192	0.683	0.425	0.687	1.017
Specific 3D parameters (baseline model)									
Burrow radius	[1]	R_b	cm	0.15	0.25	0.30	0.25	0.30	0.35
Gallery length	[5]	L_{gal}	cm	—	—	—	—	2.0	—
Eccentric distance	[5]	d	cm	—	—	—	—	0.0	—
Additional 2D parameters (extended model)									
Major radius feeding pocket	[6]	R_{fp}^{max}	cm	2.5	4.0	3.5	1.5	1.0	4.0
Additional 1D parameters (extended model)									
Diffusion enhancement factor	[6]	β	—	170	20	40	50	10	50
Restriction factor	[6]	κ	—	0.5	0.18	0.55	0.7	0.62	0.9

eccentricity d, were chosen in such a way that the feeding pocket in 3D has exactly the same location as in 2D, and that the burrow shaft remains at a sufficient distance from the core wall to avoid boundary effects.

i. Comparison of 3D and 2D models. Figure 5 shows the data profile of Br^- from one particular incubation (profile "2e" in Timmermann *et al.*, 2002), and plots the simulated profiles from the 3D and 2D baseline model alongside. The important features of the profiles are the following:

(1) A subsurface peak of Br^- builds up around the feeding depth of the lugworm, illustrating the tracer "injection" mechanism. The plume is slightly broader and shallower in the 3D baseline than in 2D baseline (max. Br^- concentration shifts from 7.3 to 7.0 mM). One explanation for this peak broadening could be the explicit appearance of the burrow in the 3D geometry. The burrow reduces the effective cross-sectional area of the core and forces flowlines to go around it. This more

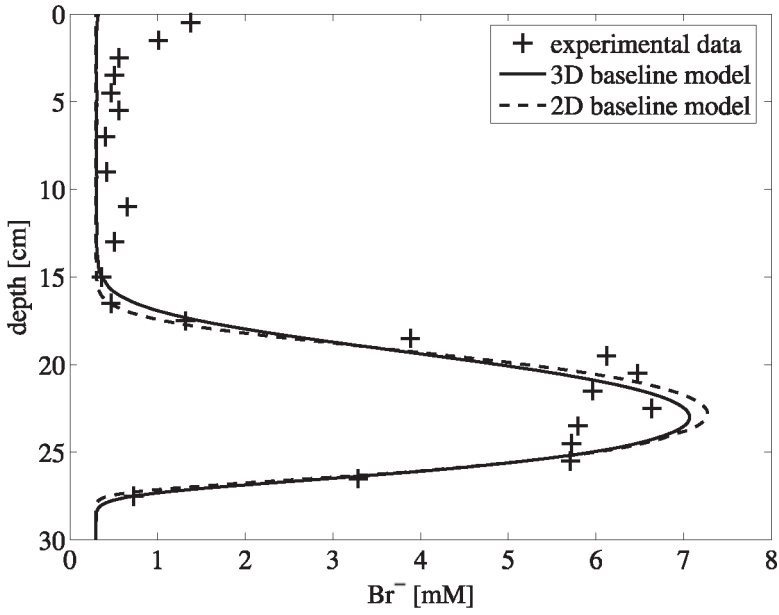

Figure 5. Numerical simulations of the Br^- injection experiment: comparison of concentration profiles generated by 3D and 2D baseline models with experimental data. Solid line = 3D model; dashed line = 2D axi-symmetric model; cross-shaped markers = experimental data (Timmermann *et al.*, 2002).

tortuous flow pattern could generate the dispersive peak-broadening observed in the depth-averaged profile of Figure 5. Another possible factor is greater numerical dispersion due to the lower resolution of the 3D finite element grid (see Fig. 2a,b). The 3D grid resolution used in the simulations was the maximal resolution we could afford in terms of internal memory available on our desktop computer platform (which still had a sizeable 2 Gb RAM). To test the influence of numerical dispersion we performed a test simulation on a coarser grid (doubling the length scale of the finite elements), and as expected, we obtained a small peak broadening (max. Br^- concentration shifts 7.0 to 6.9 mM—results not shown). From this we conclude that presence of the burrow is the dominant factor in the peak broadening going from 2D and 3D.

(2) The Br^- plume extends ~4 cm below the depth of the feeding pocket. Note that over the short time-scale of the incubation (96 min), molecular diffusion would only lead to a penetration of ~5 mm. Accordingly, the observed fast downward intrusion is not the result of diffusion, but results from downward advection of pore water.

(3) The plume is asymmetric, with the tracer penetrating the sediment faster above (~9 cm) than below (~4 cm) the feeding pocket. This faster expansion of the tracer

plume above the feeding pocket is explained in terms of the average pore water flow. The average velocity vanishes below the injection depth, but "entrains" the tracer upwards above the injection depth.

(4) The maximum of the tracer profile (~22.5 cm) does not exactly match the depth of the feeding pocket (24 cm), but occurs slightly higher up. This peak shift can be attributed to two factors. Firstly, the pumping activity of the lugworm expels bromide-free pore water from the sediment, and hence, dilutes the overlying water in the incubation chamber. Accordingly, in the course of the experiment, the concentration of the injected burrow water decreases. Secondly, the interplay of irradiation and percolation generates a three-dimensional ellipsoidal tracer plume. The depth where this ellipsoid is at its broadest does not need to coincide with the injection depth.

(5) Both the data and model profiles show a baseline concentration around C_0^s = 0.4 mmol L^{-1}, which extends above and below the subsurface peak. This baseline is due to the background concentration of bromide initially present in the pore water. Over the short time-scale of the incubation, diffusion only affects an annular zone of ~4 mm around the burrow, and this small intrusion does not markedly add to the (averaged) baseline concentration.

(6) The data show considerable "intrusion" of the tracer below the sediment-water interface (~3 cm), which is not reproduced in the model simulations. As noted above, molecular diffusion cannot explain such fast penetration of tracer (even in the absence of upward advection). The observed "anomalous" tracer intrusion could be an artifact resulting from core sectioning (when slicing the uneven sediment-water interface, tracer-rich overlying water may have been included in the top slice). Another cause might be an intensive stirring of the overlying water, which could induce advective flows in the upper sediment layer (Khalili *et al.*, 1999). However, substantial stirring speeds are needed for effects down to centimeters depth, making this factor less likely.

In conclusion, for the incubation 2e shown in Fig. 5, we find that there is very little difference between the tracer profiles generated by 3D and 2D baseline models. Both models reproduce the injected plume of bromide rather well. This similarity between 2D and 3D output is also observed for the other five incubations (a, b, c, d, f; results not shown). This suggests that (1) the flow patterns in 3D and 2D are very similar, and (2) that advection is the dominant mode of tracer transport in sediment.

ii. Comparison of 2D and 1D models. Figure 6 plots the output of 2D and 1D models next to the experimental bromide data for all six incubations in the injection dataset. The left panels compare the performance of the baseline 2D and 1D models. While the baseline 3D and 2D simulations were rather similar, there is a significant difference in the model output

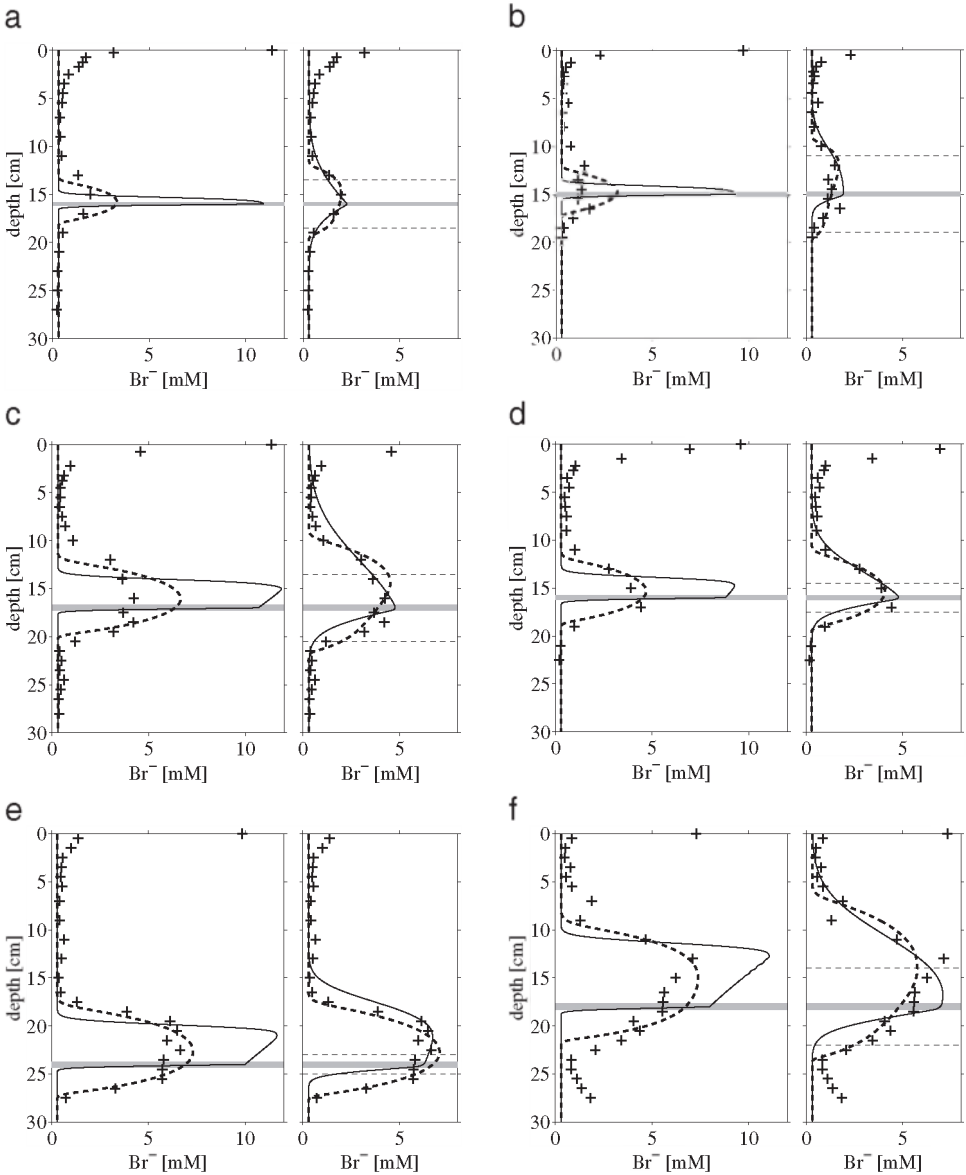

Figure 6. The tracer concentration profiles generated by baseline and extended 2D and 1D numerical models compared with experimental data. The experimental points indicated by "+" markers are from Timmermann *et al.* (2002), indices "a–f" refer to the Fig. 2a–f therein. The left panel in each image shows the output of 2D and 1D baseline models. The right panel shows the results of the 2D and 1D extended models (vertically elongated feeding pocket in 2D; restriction of the percolation area and diffusion enhancement in 1D). The grey area shows the location and width of the feeding pocket; the thin horizontal dashed lines delimits the elongated feeding pocket. Cross-shaped markers = experimental data; solid lines = 1D simulation; dashed line = 2D simulation.

between baseline 2D and 1D. In the baseline 2D profiles, the tracer plume has a typical rounded shape (broad basis, smoothened peak). The tracer penetrates considerably below the injection depth, as tracer is entrained along flowlines that irradiate downwards from the feeding pocket (Fig. 4b). In contrast, in the baseline 1D model, the tracer plume adopts the characteristic shape of a trapezoidal pulse with a small basis, steep flanks and high concentration "plateau." The concentration at the plateau linearly decreases with depth due to the dilution of the tracer in the overlying water volume. Equally, the 1D output shows a sharp decline in the tracer concentration below the injection depth. Tracer hardly penetrates downwards because there is no downward advective flow in 1D, and hence, molecular diffusion is the only transport process below the injection level. The baseline 2D model systematically generates a better fit to the experimental data than the 1D baseline model. In 3 out of 6 incubations, the 2D baseline model provides a close match of the tracer plume (Fig. 6d,e,f—left panel). In the other three simulations, the plume is wider and shallower than predicted by the baseline 2D (Fig. 6a,b,c—left panel). In contrast, in the 1D baseline model, there is always a great discrepancy between data and model output, as the modelled tracer plume is considerably sharper than as shown in the data profile.

The right panels of Figure 6 evaluate the improvement of the model fits by the extended 2D and 1D models. The parameters that are used in these simulations are given in Table 5. The 2D extended model clearly matches the data profile in those cases where the 2D baseline model shows deviations (Fig. 6a,b,c—right panel). To achieve these profiles, the minor radius $R_{fp}^{\min}$ of the elliptical feeding pocket was set to the burrow radius, while the major radius $R_{fp}^{\max}$ was tuned to obtain the best visual fit, resulting in values of 1–4 cm for $R_{fp}^{\max}$ (Table 5). Overall, differences between extended 2D and baseline 2D simulations are rather small, and as a result, the required parameter tunings are rather modest. In comparison, the difference between the model output from 1D baseline and 1D extended is much larger. While the output of the 1D baseline model strongly deviates from the data, the 1D extended models produce good fits in all simulations. However to obtain these improved fits, considerable parameter tuning was necessary, as explained in the next paragraph.

The 1D extended model emulates the 1D model of Timmermann *et al.* (2002), which incorporates three "tunable" parameters: the half-width of the injection zone R_{iz}, the diffusion enhancement factor β and the restriction factor κ. Figure 7 provides an overview of different tuning scenarios. When $\kappa = \beta = 1$ and $R_{iz} = R_b$, the extended 1D model produces the output of the baseline 1D version. When the percolation area is decreased, i.e. $\kappa < 1$, one observes a broadening of the tracer plume, though solely above the injection depth. When the half-width of the injection zone is increased, i.e. $R_{iz} > R_b$, one obtains a similar peak-broadening, though now above and below the injection depth. In both scenarios however, the plume retains the sharp pulse-like shape of the original baseline 1D profile, i.e., a flat plateau with steep flanks. Only when dispersion is strongly enhanced, i.e. $\beta \gg 1$, one obtains the broad, smoothly varying tracer plume as in the data profile. In Timmermann *et al.* (2002), the parameters κ, R_{iz} and β were simultaneously adjusted to

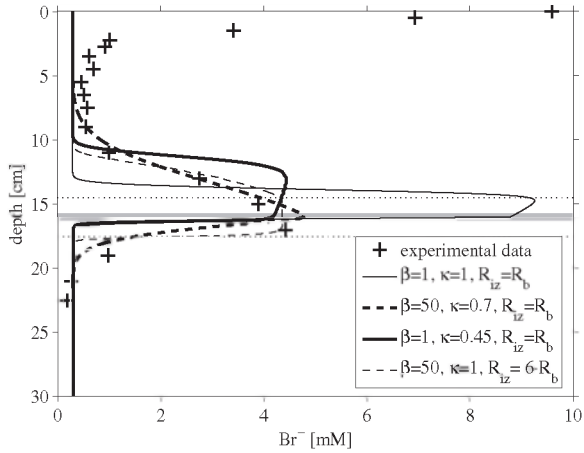

Figure 7. Exploration of several tuning scenarios for the extended 1D model. Three different tuning parameters can be altered: the half-width of the injection zone R_{iz}, the percolation factor κ, and the diffusion enhancement factor β. Best fits are shown for combinations of these parameters. The experimental data are the same as in Fig. 6d.

obtain fits of the extended 1D model. Our simulations (Fig. 7) show that this might actually be an "overtuning" of the model. The adaptation of two parameters (i.e. a combination of one "peak-broadening" parameter, either κ or R_{iz}, together with the "peak-smearing" parameter β) seems sufficient to obtain good fits of the 1D model to the data. This is shown in the right panels of Figure 6, where tracer profiles are fitted by simultaneously restricting the percolation area (adapting κ) and introducing additional "artificial" dispersion (tuning β). The reduction of the percolation zone that is needed is quite significant, and ranges from 10% (Fig. 6f) up to 82% (Fig. 6b). Similarly, to acquire reasonable fits, the natural rate of dispersion has to be scaled by one or two orders of magnitude, i.e. the β-factor ranged from 10 to 170 (Table 5). So, while the 2D extended model only incorporates the "natural" hydrodynamic dispersion, the 1D extended model requires the inclusion of significant "artificial" dispersion.

c. Flushing simulations

The "flushing" dataset consists of two separate flushing experiments, where the evolution of the tracer (NO_3^-) concentration in the overlying water of the incubation chamber was monitored continuously. The experimental conditions in the two experiments are similar (Table 6), apart from two parameters, i.e., the lugworm's feeding depth H_{fp} and pumping rate Q. In core 1, a relatively large lugworm was introduced (expected to show a large pumping rate) and no attempt was made to control its feeding depth. Upon introduction, visual inspection revealed that the lugworm established its burrow gallery close to the bottom of the core. In core 2, a smaller individual was introduced (with a smaller pumping rate), which was prohibited from

Table 6. Summary of parameters used in the model simulations of the "flushing" experiments.

Core set-up			NO_3^- (C#1)	NO_3^- (C#2)
Core diameter	$2R_c$	cm	11.2	11.2
Sediment depth	H_s	cm	8.5	10
Height overlying water column	H_w	cm	3.05	3.05
Experimental conditions				
Temperature	T	°C	15	15
Salinity	S	‰	30	30
Porosity	ϕ	—	0.68	0.65
Median grain size	$\bar{r}$	μm	220	220
Incubation parameters				
Incubation time	t_{final}	min	>1200	>1500
Initial concentration overlying water	C_0^w	μM	0	0
Initial concentration pore water	C_0^s	μM	385	364
***A. marina* parameters (common to 1D/2D/3D baseline)**				
Depth feeding pocket	H_{fp}	cm	7	5
Radius feeding pocket	R_{fp}	cm	0.25	0.25
Burrow consumption factor	λ	—	1	1
Pumping rate	Q	$cm^3\ min^{-1}$	1.3	0.3
***A. marina* parameters (specific for 3D baseline)**				
Burrow radius	R_b	cm	0.3	0.3
Burrow radius	L_{gal}	cm	2	2
Eccentric distance feeding pocket	d	cm	0	0

burrowing deeper than 5 cm by placing a mesh at that depth. It was observed that the lugworm burrowed until it encountered the obstructing mesh.

The tracer evolution in the water phase of core 1 (C1, big worm) shows a relatively fast release of NO_3^- from the sediment. The system reaches a steady state after about 800 minutes, when pore water and overlying water are completely mixed to a concentration of 252 μmol L^{-1}. In contrast, core 2 (C2, small worm) shows a more gradual increase of the tracer concentration in the overlying water, indicating a slower release of nitrate from the sediment. At the end of the incubation (after 1500 min), the concentration is still rising, indicating that pore water and overlying water are not yet fully mixed. The most noticeable difference between core 1 and 2 is the non-monotonic increase of the tracer concentration in core 1. On the way to steady state, at about 300 minutes, the NO_3^- concentration overshoots the final steady state value. Although the "overshoot" is small, its magnitude is well above the analytical error of the nitrate electrode. It is not an artifact, but results from the mechanism of lugworm bio-irrigation. During the initial stage of the incubation, the lugworm expels a volume of high NO_3^- pore water from the sediment, which temporarily causes the concentration in the overlying water to exceed the final equilibrium value. This overshoot in the data turned out to be an excellent feature to test the response of the various models.

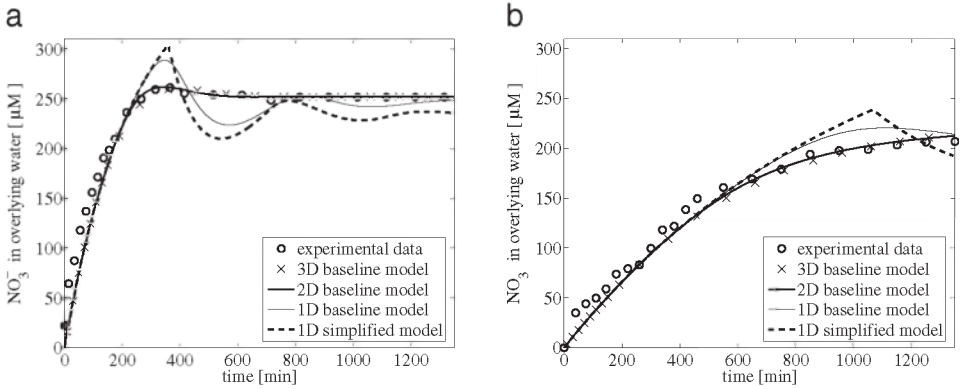

Figure 8. Dynamical simulation of NO_3^- flushing experiment: evolution of the nitrate concentration in overlying water with time. (a) Core #1: the lugworm is allowed freely to establish its burrow. (b) Core #2: the depth of burrowing is restricted by a wire mesh placed at 5 cm below the sediment surface.

Figure 8 compares how the different models reproduce the evolution of the NO_3^- concentration in the overlying water. Again parameters were constrained with measurements as much as possible. In the 1D and 2D baseline models, 13 out of 14 parameter values could be fixed *a priori* (Table 6), the pumping rate Q remaining as a single fitting parameter. Using the 2D baseline model, the pumping rates in C1 and C2 were respectively estimated as 1.3 and 0.3 $cm^3\ min^{-1}$. These values were then used in the simulations with the other models, and reflect very well the difference in size of the lugworms that were used in the incubations. For the 3D baseline model, three specific parameters were additionally needed (Table 6). Only one of them, the burrow radius, could be constrained by data (R_b = 0.3 cm in both C1 and C2). Given the rather small core size, the length of the gallery was estimated to be small (L_{gal} = 2 cm), and the feeding pocket was assumed to be in the center of the core (d = 0 cm).

The modeling results again show a clear contrast between 3D/2D models on the one hand, and 1D models on the other hand (Fig. 8). Effectively, the response of the 3D and 2D baseline model cannot be distinguished on the resolution of the graph. In addition, the output of both 3D and 2D models closely matches the experimental data. Especially the overshoot mechanism in core 1 is excellently reproduced, confirming the mechanistic explanation of this particular data feature. In contrast, the 1D baseline simulation significantly overestimates this overshoot feature. Overall, the 1D baseline model produces a "tortuous" response: the tracer concentration shows pronounced oscillations, which are gradually dampened on the way to equilibrium. For comparison, we also plotted the response of the 1D simplified model, in which $C^{ow}(t)$ exhibits a sharp maximum when the injected water reaches the sediment-water interface for the first time. The 1D simplified model can be regarded as the baseline 1D without hydrodynamic dispersion. Overall, these

two 1D models generate a comparable response, which significantly deviates from the data profile. The inclusion of hydrodynamic dispersion as in the 1D baseline model only slightly smoothens the oscillations. In contrast, the 2D/3D baseline model generates a "flattened" response, in which all oscillations have been smoothened, but for the first overshoot in core 1. This smoothening is explained by the irradiative form of the flowline pattern in 2D and 3D. This emphasizes that the shape of the advective flow pattern, and in particular advective flows beneath the feeding depth, are crucial in simulating lugworm irrigation.

4. Discussion

a. Optimal complexity in models of lugworm bio-irrigation

Lugworms actively ventilate their J-shaped burrows, and this results in a characteristic mode of bio-irrigation as revealed in closed-chamber incubations using inert solute tracers (Rasmussen *et al.*, 1998; Timmermann *et al.*, 2002; Meysman *et al.*, 2006). This lugworm "signature" produces two specific signals: (1) the build-up of a subsurface "tracer plume" due to the injection of burrow water at depth, and (2) a characteristic—sometimes oscillatory—evolution of the tracer concentration in the overlying water column, which results from the intake of fresh water into the burrow and the concomitant expulsion of pore water across the sediment water interface. Here, we have explored a range of mathematical models that simulate these two signals. To reinforce the mechanistic character of these simulations, model parameters were fixed *a priori* based on experimental data and commonsensical constraints. Our main objective was to assess the minimal model complexity required to accurately simulate lugworm bio-irrigation.

i. Comparison 3D and 2D baseline models. Three different aspects within our simulations indicate that the 3D micro-environment model, with a full description of the burrow geometry, can be readily simplified to a 2D axi-symmetric description that only incorporates the feeding pocket. (1) The 3D flow pattern tends to be radially symmetric (Fig. 4a), and is very similar to the flowline pattern generated by the simplified 2D model (Fig. 4b). Accordingly, the 3D flow pattern is not significantly influenced by the presence of the burrow. The burrow only forms a small obstacle, and is easily circumvented by the flowlines that rise to the sediment-water interface. (2) Tracer profiles generated by the 3D model are nearly identical to those obtained from the 2D model, when laterally averaged over the sediment domain (Fig. 5). (3) Flushing simulations reveal a similar response of the tracer concentration in the overlying water in 3D and 2D models (Fig. 8). Overall, the similarity of the various 3D and 2D simulations indicates that a "full" description of the 3D burrow geometry adds little value in terms of mechanistic modeling, justifying the 2D pocket injection approach advanced by Meysman *et al.* (2006). The implications for both modeling and experimental studies are considerable. By moving from 3D to 2D, one can drastically reduce the required computational resources without compromising the predic-

tive power of the model. Equally, in laboratory and field experiments, one can significantly reduce the number of parameters that need to be measured (from 16 in 3D to 13 in 2D; Tables 2, 6).

ii. Comparison of 2D and 1D models. In terms of the number of parameters, a further simplification from 2D to 1D does not result in a further decrease in complexity (both 2D and 1D baseline models contain 13 parameters; Table 2). On the contrary, the extended 2D model contains even 1 parameter less than the extended 1D model. When comparing the Br^- profiles produced by these extended 2D and 1D models, it appears that both models produce equally good fits (Fig. 6). This goodness of fit is however a deceiving criterion for the mechanistic basis and predictive capacity of these models. To this end, one should compare the performance of the extended versions (with tuning parameters) to that of the baseline versions (without adjustable parameters). In the 2D case, the baseline model already provides a very good fit to both Br^- and NO_3^- data (Figs. 6 and 8), indicating that the mechanism of lugworm bio-irrigation is appropriately captured. To improve fits, the 2D extended version contains one extra tunable parameter, which requires modest adjustment. In contrast, in the 1D case, the "unadjusted" baseline simulations significantly misrepresent the experimental data (Figs. 6 and 8), pointing towards a poor mechanistic basis. To obtain decent fits in 1D, two fitting parameters needed considerable adjustment: the diffusion enhancement factor β and the percolation restriction factor κ. Table 5 illustrates that the fitted values for β and κ show considerable variation between profiles, which is remarkable, given that the Br^- incubation experiments were replicates with similar-sized lugworms. A closer inspection of the β and κ parameters reveals the origin of this variation.

Firstly, fitted values for the diffusion enhancement factor β are very high, ranging from 10 to 170 (Table 5). Based on these high values, Timmermann *et al.* (2002) concluded that a strong diffusive transport mechanism must be operating, and invoked porewater mixing due to meiofauna and hydrodynamic dispersion as possible explanations. However, neither mechanism seems a plausible explanation for the high β values. Diffusion enhancement by meiofauna is only important at high meiofaunal densities (Glud and Fenchel, 1999), and reported enhancement factors are always in the modest range of 2 to 5 (Aller, 2001). A similar conclusion holds for hydrodynamic dispersion. If one uses the pumping rates in Table 5, one can calculate average pore water velocities $v = Q/(\phi A_c)$ in the range of 6–34 m yr^{-1}, and grain scale Péclet numbers ranging from 0.9–5. Applying formula (12) one obtains average D_L/D_{mol} values ranging from 0.4 to 3.5, pointing towards a modest diffusion enhancement due to hydrodynamic dispersion. Accordingly, we conclude that enhancement due to meiofauna or dispersion does not explain the large β values fitted by the extended 1D model (Table 5).

Effectively, our 2D and 3D model simulations contradict that strong diffusive transport is acting: they provide a good fit to the data without including additional diffusion on top of the standard dispersion relations (12)–(13). Adopting a similar calculation as above

(replacing A_c with the surface area of a suitable sphere around the feeding pocket), D_L/D_{mol} values right at the surface of the feeding pocket are huge (range 600–5000), but very quickly drop at a distance of 1 cm (range 2–15). Therefore, hydrodynamic dispersion is only important in a small halo around the feeding pocket where velocities are high. As a result, lugworm pumping appears to induce velocities that are high enough, so that advective tracer transport clearly dominates molecular diffusion on the decimeter scale of the bio-irrigated zone. But, velocities are still low enough so that the level of hydrodynamic dispersion remains low (the exponent in expressions (11) and (12) is larger than 1, so dispersion becomes more important at higher velocities). As a result, possible non-linear effects of transient pumping on dispersion appear to be also justifiably neglected.

So in summary, the shape of the tracer plumes (Figs. 5, 6, 7) and the evolution of the tracer concentration in the overlying water (Fig. 8) are principally determined by pore water advection, with only a minor influence of diffusive/dispersive processes. This "advective" control does not contradict the high "diffusive" β values fitted by the 1D model. The observed "dispersive" spreading in the 1D tracer data (Fig. 6) basically results from the 3D diverging flow around the feeding pocket. In this "irradiation zone," pore water packages are transported in various directions along different flowlines, and so, tracer is also transported *downwards* from the injection zone. By definition, 1D models cannot account for radial variation in pore water velocities, and hence, from the perspective of the 1D model, no advective transport occurs beneath the injection zone. Consequently, any fast appearance of tracer beneath the injection zone has to be accounted for by an enhanced "mixing" of the pore water. This way, the enhanced diffusion in the 1D model (16) appears to be a true example of a "modeling artifact": strong diffusive transport must be included in 1D to emulate the solute spreading induced by advection in 3D.

In a similar fashion, one can investigate the mechanistic nature of the percolation factor κ. In the extended 1D model, the κ factor basically determines the rate of spreading of the tracer plume. For the same pumping rate Q, smaller κ values will generate a faster flow within the percolation zone, thus increasing the width of the simulated 1D tracer plume. The question then is whether this plume spreading is really due to preferential flow in a percolation zone (see discussion in Meysman *et al.*, 2005). Fitted κ values range from 0.18 to 0.9, implying that the area of the apparent percolation zone A_{pz} differed more than five-fold between cores (Table 5). It is questionable that similar-sized lugworms would create such widely different percolation zones under exactly the same experimental conditions. In the extended 2D model, a very different mechanism is proposed to enhance the spreading of the plume as compared to the 1D model. The feeding pocket is elongated, thus resulting in a larger depth interval over which burrow water is injected (Fig. 6 shows the fits with and without this tuning parameter). This vertical elongation of the feeding pocket ranges from 1 to 4 cm (Table 5), and this range might reflect actual lugworm repositioning distances and feeding pocket shapes.

Overall, the above model analysis illustrates the poor mechanistic basis of the diffusion enhancement factor β and a percolation restriction factor κ in the 1D model formulation

(15). This ad-hoc character is emphasized by the fact that neither parameters showed any allometric relation with the size of the organisms (Timmermann *et al.*, 2002). This contrasts strongly with the estimated pumping rate Q, which showed a strong allometric relationship with body size (Timmermann *et al.*, 2002). This indicates that the pumping rate can be used to make predictions for other sites with different lugworm populations, which is not the case for diffusion enhancement factor β and a percolation restriction factor κ.

b. The usefulness of 1D bio-irrigation formulations?

A pertinent question is how relevant our observations on lugworm models are for bio-irrigation in general. Effectively, present-day bio-irrigation models exemplify an interesting paradox, where the complexity of the natural process sharply contrasts with the simplicity of the model description. Although bio-irrigation forms a complex three-dimensional phenomenon, it is mostly described via 1D process models, either (1) enhanced advection, i.e., increase the pore water flow velocity with a factor due to biological activity (Hammond and Fuller, 1978; Benoit *et al.*, 1991; Timmermann *et al.*, 2002), (2) enhanced diffusion, i.e. increase the diffusion coefficient with a factor due to bio-irrigation (Vanderborght *et al.*, 1977; Aller and Yingst, 1985; Forster *et al.*, 1995; Berg *et al.*, 2001; Timmermann *et al.*, 2002), or (3) enhanced reaction, i.e. include bio-irrigation by means of a non-local exchange formulation that functions as an apparent reaction term (McAffrey *et al.*, 1980; Emerson *et al.*, 1984; Christensen *et al.*, 1984; Boudreau, 1984; Meile and Van Cappellen, 2003). The popularity of these 1D models is presumably because of two main reasons. One, pore water retrieval by core sectioning produces laterally averaged concentrations of solutes, and hence, delivers data in a one-dimensional format. Two, 1D bio-irrigation representations are compellingly simple in application. They condense the bio-irrigation phenomenon to a single parameter, which allows a straightforward comparison between sites. Over the past two decades, these 1D representations of bio-irrigational transport have been widely incorporated in standard reactive transport models of sediment biogeochemistry (Soetaert *et al.*, 1996; Boudreau, 1996a; Van Cappellen and Wang, 1996; Meysman *et al.*, 2003; Berg *et al.*, 2003).

Given their widespread use, a crucial question is how "accurate" these standard 1D bio-irrigation formulations are. In this regard, there are two troublesome aspects, which have received little attention. Firstly, 1D bio-irrigation models (deceivingly) radiate confidence, because they are able to accurately reproduce observed mass fluxes and/or concentration profiles for a single constituent, typically a conservative tracer (e.g. Benoit *et al.*, 1991; Wallmann *et al.*, 1997; Schluter *et al.*, 2000; Meile *et al.*, 2001; Timmermann *et al.*, 2002; Forster *et al.*, 2003). But as noted by Aller (2001), this goodness of fit of a given 1D expression constitutes a weak proxy for its mechanistic character and predictive power. Pure mathematically, one can reproduce virtually any 1D tracer profile by suitably parametrizing a single depth-dependent transport mechanism in an uncoupled 1D transport equation. Using a systematic identifiability and uncertainty analysis of parameters in 1D

models, Andersson *et al.* (2006) showed that attenuation constants, which regulate the depth dependency of irrigation parameters, are particularly insensitive. This "unconstrained" nature of 1D bio-irrigation formulations makes that excellent fits do not warrant confidence in the underlying physical mechanism. Secondly, there is a crucial weakness in the three step procedure by which bio-irrigation is presently incorporated into biogeochemical models. (1) A tracer experiment is carried out with a specific conservative irrigation tracer. (2) A 1D irrigation parameter is calibrated by appropriately fitting a 1D model to the tracer profile. (3) This irrigation parameter value is then included in the transport equation of all pore water solutes. The danger is in the last step: one implicitly assumes that the mathematical 1D bio-irrigation formulation is "unconditionally valid," in other words, that it adequately captures the physical mechanism of bio-irrigation.

Recently, this implicit assumption has been put to the test for the "diffusive" tube-irrigation mechanism of bio-irrigation (Grigg *et al.*, 2005; Meile *et al.*, 2005). Numerical simulation experiments were performed using Aller's 2D tube-irrigation model to create a virtual dataset. These "generated" data were then fitted with solutions of the classical 1D source-sink description $\Gamma = \alpha(C_0 - C(z))$, where α is the non-local irrigation coefficient, C_0 is the concentration of the overlying water, and C is the laterally averaged concentration at depth. The results of this exercise are rather disturbing for the validity of the widely used non-local exchange formulation. Grigg *et al.* (2005) concluded that under field-type biogeochemical conditions (multiple reactive species, coupled non-linear kinetics) the 1D non-local formulation performs poorly, wrongly predicting averaged reaction rates and fluxes across the sediment-water interface. The crucial weakness of the non-local 1D model is that by definition, it cannot capture the actual driving force of "diffusive" bio-irrigation: the presence of radial concentrations gradients near the burrow wall. In a similar study of multi-species biogeochemistry, Meile *et al.* (2005) confirmed that when fitting 1D profiles to the output of the 2D model, the fitted α values are strongly species-dependent. Furthermore, both Andersson *et al.* (2006) and Meile *et al.* (2005) showed that even for inert solutes, the determination of α values can be ambiguous. Simulating closed incubation experiments, the 1D irrigation coefficient α showed an artificial dependence on the incubation time, falsely suggesting that the intensity of irrigation changes over time. The numerical experiments by Grigg *et al.* (2005) and Meile *et al.* (2005) reveal that the third step in the classical procedure of modeling bio-irrigation is truly problematic. When all pore water solutes are assigned the same α value, as is traditionally done in 1D diagenetic models (Soetaert *et al.*, 1996; Boudreau, 1996a; Van Capellen and Wang, 1996; Meysman *et al.*, 2003), one may expect significant errors in the predicted rates and fluxes.

In this study, we have carried out a similar critical model evaluation of 1D models, though now for the advective mechanism of bio-irrigation that occurs in sandy environments. Our analysis is based on the comparison of 2D and 1D simulation output, as in Grigg *et al.* (2005) and Meile *et al.* (2005), but also by comparing 2D and 3D output, and on the confrontation of the model output with two separate types of experimental data

(flushing and intrusion experiments). Our results show that one should be very careful when applying 1D models to advective bio-irrigation in permeable sediments. 1D models do not accurately describe the three-dimensional flow pattern in the sediment. This 3D flow pattern can be simplified to an axial 2D symmetry without major deviations. However, upon further averaging to a 1D representation, one loses all directional information on the flow pattern, and hence, the 1D model does not capture the essential process that drives bio-irrigation. As a result, calibrated values of 1D parameters have a strong ad-hoc character, and typically show strong variation among replicate experiments. Although not tested in this study, when combining 1D bio-irrigation models in sandy sediments with multi-species biogeochemistry, we expect similar anomalies as those recorded by Grigg *et al.* (2005) and Meile *et al.* (2005). When transferring 1D irrigation parameters from the inert tracer to other solutes with a different biogeochemistry, there is a considerable chance of making invalid predictions about fluxes and rates.

5. Conclusion

In nature, bio-irrigation forms a complex three-dimensional phenomenon: both advective and diffusive pore water transport may result from burrow ventilation, and this transport is intrinsically dependent on the 3D geometry of the burrow structures. Over the last few decades biogeochemical modellers have explored various approaches on how to deal with this complexity. Polarizing this debate, one can confront two extreme and opposite views: the "complex 3D" view versus the "simple 1D" view. A proponent of the former would argue that a complex process like bio-irrigation can only be but understood by equally complex models. In other words, quantification of bio-irrigation requires a firm grasp on all complexity involved (measure and map the full 3D burrow geometry, heterogeneity in the sediment properties, transient pumping pattern, etc). Oppositely, the "simple 1D" proponent would argue that bio-irrigation is just a too complex process, governed by too many unknown parameters, which introduces too many uncertainty. As a result, there is no benefit in exploring complex mechanistic models—they would not work anyway. Therefore, one should stick to simplified empirical 1D descriptions with calibrated parameters, which are easy to use and offer a straightforward comparison between sediment environments.

This case study of lugworm bio-irrigation provides a clear set of counter arguments for either of these two perspectives. Lugworm bio-irrigation is dominated by advective transport, and hence, a good mechanistic model should properly represent the flow pattern in the pore water. In the spirit of Einstein, we show that "things can be made simple," and suitable results and insight can be obtained by means of a micro-environment model with strongly simplifying assumptions (steady pumping rate, no heterogeneity in sediment properties, neglect of burrow geometry, and hence, simplifying 3D to 2D by assuming radial symmetry). However, a further simplification from 2D to 1D seems to go beyond Einstein's "not simpler than that." By their very nature, 1D formulations cannot capture the essential mechanism that drives bio-irrigation: radial concentration gradients for the "diffusive" tube-irrigation mechanism (Grigg *et al.*, 2005; Meile *et al.*, 2005), and flow patterns for the "advective" pocket-injection mechanism (this

work). As a result, present 1D bio-irrigation formulations should be used with caution, and seem to contribute little to our understanding of the coupling between transport, geochemistry and benthic biology. The connection of 1D parameters to the underlying biology is weak, so that extrapolation to other conditions (e.g. sediments with similar organisms at different densities) becomes problematic. Facing this problem, biogeochemical modellers are confronted with a real challenge. There is a clear need for simplified 1D models in quantitative biogeochemistry, which is computationally intensive even with present day computing facilities (multi-species non-linear kinetics, coupling to general circulation models). Therefore, a real challenge is to further investigate when and why 1D bio-irrigation descriptions fail, and if possible, how they can be rescued.

Acknowledgments. We thank an anonymous referee, Christof Meile and the editor, Don Rice, for their valuable and constructive comments, which greatly benefited this manuscript. This research was supported by grants from the EU (NAME project, EVK#3-CT-2001-00066, COSA project, EVK#3-CT-2002-00076) and a PIONIER from the Netherlands Organization for Scientific Research (NWO, 833.02.2002). This is publication 3806 of the Netherlands Institute of Ecology (NIOO-KNAW).

APPENDIX

Analytical solution to 1D tracer flushing problem

Consider a 1D advective bio-irrigation problem with localized (point) source in the absence of diffusion. The pore water is initially uniformly loaded with passive tracer, the overlying water is clean. The problem is linear in the tracer concentration, so we can assume the following initial conditions: at time $t = 0$ the tracer concentration in the sediment is $C_0^s = 1$ while in the water column $C_w^0 = 0$. The upward actual pore water velocity (the speed of the concentration front propagation) u can be expressed via the pumping rate Q and horizontal cross-section of the sediment core A_c as

$$u = \frac{Q}{A_c \phi} \tag{A18}$$

The characteristic time during which the pore water is completely refreshed is

$$\tau = \frac{H_{fp}}{u} \tag{A19}$$

If only advective transport takes place we can formulate the problem only in terms of the tracer concentration in the overlying water column, which for brevity will be denoted as $y(t) \equiv C^w(t)$. During the first period $0 \leq t \leq \tau$ when the water exiting the sediment column still has the initial concentration $C_0^w = 1$ the evolution of $y(t)$ is described by the first order ordinary differential equation

$$\frac{dy}{dt} = -ay + a, \text{ where } a = \frac{\phi u}{H_w} \tag{A20}$$

The general solution of the first-order linear differential equation

$$y' + P(t)y = Q(t) \tag{A21}$$

is given by the formula (Bronshtein *et al.*, 2003):

$$y = \exp\left(-\int Pdt\right)\left[\int Q\exp\left(\int Pdt\right)dt + C\right] \tag{A22}$$

In the case of the equation (A20) $P(t) \equiv a$ and $Q(t) \equiv a$, the solution takes form

$$y(t) = e^{-at}(C + e^{at}) = 1 + Ce^{-at}. \tag{A23}$$

Applying the initial condition $y(0) = 0$ we find that $C = 1$ and, as a result the solution is

$$y(t) = 1 - e^{-at},\ 0 \le t \le \tau. \tag{A24}$$

At the moment $t = \tau$ the front of the injected water reaches the sediment-water interface, so the concentration of the water leaving the sediment is not constant any more. In the absence of diffusion the water leaving the sediment at the moment t is the same water that was injected into the sediment at the moment $t' = t - \tau$, so the concentration of the tracer corresponds to $y(t') = y(t - \tau)$. The equation (A20) now is changed into

$$\frac{dy(t)}{dt} = -ay(t) + ay(t - \tau). \tag{A25}$$

For the time interval $\tau \le t \le 2\tau$ the argument of the second function in the right-hand side of the equation (A25) belongs to the first period ($0 \le t - \tau \le \tau$). Consequently, $y(t - \tau)$ is described by the expression (A24). Using formula (A22) (Bronshtein *et al.*, 2003) and demanding the continuity at $t = \tau$, one obtains the solution:

$$y(t) = 1 - e^{-at} - a(t - \tau)e^{-a(t-\tau)},\ \tau \le t \le 2\tau. \tag{A26}$$

Repeating the same procedure further, we can guess, and by means of mathematical induction prove, that the general solution for all values of t is given by the formula

$$y(t) = 1 - e^{-at}\sum_{j=0}^{n}\frac{a^j e^{ja\tau}}{j!}(t - j\tau)^j,\ n\tau \le t \le (n+1)\tau,\ n = 0, 1, 2, \ldots \tag{A27}$$

Finally for arbitrary values of (initially uniform) tracer concentrations C_0^s and C_0^w in the sediment layer and water column respectively the solution takes form

$$C^w(t) = C_0^s + (C_0^w - C_0^s)e^{-at}\sum_{j=0}^{n}\frac{a^j e^{ja\tau}}{j!}(t - j\tau)^j,\ n\tau \le t \le (n+1)\tau,\ n = 0, 1, 2, \ldots \tag{A28}$$

REFERENCES

Aller, R. C. 1980. Quantifying solute distributions in the bioturbated zone of marine-sediments by defining an average micro-environment. Geochim. Cosmochim. Acta, *44*, 1955–1965.

—— 2001. Transport and reactions in the bioirrigated zone, *in* The Benthic Boundary Layer, B. P. Boudreau and B. B. Jorgensen, eds., Oxford University Press, 269–301.

Aller, R. C. and J. Y. Aller. 1998. The effect of biogenic irrigation intensity and solute exchange on diagenetic reaction rates in marine sediments. J. Mar. Res., *56*, 905–936.

Aller, R. C. and J. Y. Yingst. 1985. Effects of the marine deposit-feeders *Heteromastus filiformis* (Polychaeta), *Macoma balthica* (Bivalvia), and *Tellina texana* (Bivalvia) on averaged sediment solute transport, reaction rates and microbial distribution. J. Mar. Res., *43*, 615–645.

Anderson, J. G. and P. S. Meadows. 1978. Microenvironments in marine sediments. Proc. Roy. Soc. Edinburgh Sect. B, *76*, 1–16.

Andersson, J. H., J. J. Middelburg and K. Soetaert. 2006. Identifiability and uncertainty analysis of bio-irrigation rates. J. Mar. Res., *64*, 407–429.

Archer, D. and A. Devol. 1992. Benthic oxygen fluxes on the Washington shelf and slope—A comparison of *in situ* microelectrode and chamber flux measurements. Limnol. Oceanogr., *37*, 614–629.

Bear, J. and Y. Bachmat. 1991. Introduction to Modeling of Transport Phenomena in Porous Media, Kluwer Academic Publishers, 553 pp.

Benoit, J. M., T. Torgersen and J. O'Donnell. 1991. An advection diffusion-model for Rn-222 transport in near-shore sediments inhabited by sedentary polychaetes. Earth, Planet. Sci. Lett., *105*, 463–473.

Berg, P., S. Rysgaard, P. Funch and M. K. Sejr. 2001. Effects of bioturbation on solutes and solids in marine sediments. Aquat. Microb. Ecol., *26*, 81–94.

Berg, P., S. Rysgaard and B. Thamdrup. 2003. Dynamic modeling of early diagenesis and nutrient cycling. A case study in an Arctic marine sediment. Am. J. Sci., *303*, 905–955.

Beukema, J. J. and J. De Vlas. 1979. Polulation parameters of the lugworm, *Arenicola marina*, living on tidal flats in the Dutch Wadden Sea. Neth. J. Sea Res., *13*, 331–353.

Boudreau, B. P. 1984. On the equivalence of nonlocal and radial-diffusion models for porewater irrigation. J. Mar. Res., *42*, 731–735.

—— 1996a. A method-of-lines code for carbon and nutrient diagenesis in aquatic sediments. Comput. Geosci., *22*, 479–496.

—— 1996b. The diffusive tortuosity of fine-grained unlithified sediments. Geochim. Cosmochim. Acta, *60*, 3139–3142.

Boudreau, B. P. and R. L. Marinelli. 1994. A modeling study of discontinuous biological irrigation. J. Mar. Res., *52*, 947–968.

Bronshtein, I. N., K. A. Semendyayev, G. Musiol and H. Muehlig. 2003. Handbook of Mathematics, Springer, 1153 pp.

Cadée, G. C. 1976. Sediment reworking by *Arenicola marina* on tidal flats in the Dutch Wadden Sea. Neth. J. Sea Res., *10*, 440–460.

Christensen, J. P., A. H. Devol and W. M. Smethie. 1984. Biological enhancement of solute exchange between sediments and bottom water on the Washington shelf. Cont. Shelf Res., *3*, 9–23.

Davis, R. B. 1974. Tubificids alter profiles of redox potential and pH in profundal lake sediments. Limnol. Oceanogr., *19*, 342–346.

Emerson, S., R. Jahnke and D. Heggie. 1984. Sediment-water exchange in shallow-water estuarine sediments. J. Mar. Res., *42*, 709–730.

Forster, S., G. Graf, J. Kitlar and M. Powilleit. 1995. Effects of bioturbation in oxic and hypoxic

conditions—A microcosm experiment with a North-Sea sediment community. Mar. Ecol. Prog. Ser., *116*, 153–161.

Forster, S., A. Khalili and J. Kitlar. 2003. Variation of nonlocal irrigation in a subtidal benthic community. J. Mar. Res., *61*, 335–357.

Foster-Smith, R. L. 1978. An analysis of water flow in tube-living animals. J. Exp. Mar. Biol. Ecol., *34*, 73–95.

Freeze, R. A. and J. A. Cherry. 1979. Groundwater, Prentice Hall, 604 pp.

Furukawa, Y., S. J. Bentley and D. L. Lavoie. 2001. Bioirrigation modeling in experimental benthic mesocosms. J. Mar. Res., *59*, 417–452.

Glud, R. N. and T. Fenchel. 1999. The importance of ciliates for interstitial solute transport in benthic communities. Mar. Ecol. Prog. Ser., *186*, 87–93.

Grigg, N. J., B. P. Boudreau, I. T. Webster and P. W. Ford. 2005. The nonlocal model of porewater irrigation: limits to its equivalence with a cylinder diffusion model. J. Mar. Res., *63*, 437–455.

Gust, G. and J. T. Harrison. 1981. Biological pumps at the sediment-water interface: mechanistic evaluation of the alpheid shrimp *Alpheus mackayi* and its irrigation pattern. Mar. Biol., *64*, 71–78.

Hammond, D. E. and C. Fuller. 1979. The use of radon-222 as a tracer in San Francisco Bay, *in* San Francisco Bay: The Urbanized Estuary, T. J. Conomos, ed., American Association for the Advancement of Science, 213–230.

Hylleberg, J. 1975. Selective feeding by *Abarenicola pacifica* with notes on *Abarenicola vagabunda* and a concept of gardening in lugworms. Ophelia, *14*, 113–137.

Jones, S. E. and C. F. Jago. 1993. In situ assessment of modification of sediment properties by burrowing invertebrates. Mar. Biol., *115*, 133–142.

Khalili, A., A. J. Basu, U. Pietrzyk and B. B. Jorgensen. 1999. Advective transport through permeable sediments: a new numerical and experimental approach. Acta Mech., *132*, 221–227.

Koretsky, C. M., C. Meile and P. Van Cappellen. 2002. Quantifying bioirrigation using ecological parameters: a stochastic approach. Geochem. Trans., *3*, 17–30.

Kruger, F. 1971. Bau und leben des wattwurmes *Arenicola marina*. Helgol. Meeresunters., *22*, 149–200.

Lichtner, P. C. 1996. Continuum formulation of multicomponent-multiphase reactive transport, *in* Reactive Transport in Porous Media, P. C. Lichtner, C. C. Steefel, and E. H. Oelkers, eds., The Mineralogical Society of America, 1–82.

Marinelli, R. L., C. R. Lovell, S. G. Wakeham, D. B. Ringelberg and D. C. White. 2002. Experimental investigation of the control of bacterial community composition in macrofaunal burrows. Mar. Ecol. Prog. Ser., *235*, 1–13.

McCaffrey, R. J., A. C. Myers, E. Davey, G. Morisson, M. Bender, N. Luedtke, D. Cullen, P. Froelich and G. Klinkhammer. 1980. The relation between pore water chemistry and benthic fluxes of nutrients and manganese in Narragansett Bay. Limnol. Oceanogr., *25*, 31–44.

Meadows, P. S. and J. Tait. 1989. Modification of sediment permeability and shear-strength by 2 burrowing invertebrates. Mar. Biol., *101*, 75–82.

Meile, C., P. Berg, P. Van Cappellen and K. Tuncay. 2005. Solute-specific pore water irrigation: implications for chemical cycling in early diagenesis. J. Mar. Res., *63*, 601–621.

Meile, C., C. M. Koretsky and P. Van Cappellen. 2001. Quantifying bioirrigation in aquatic sediments: an inverse modeling approach. Limnol. Oceanogr., *46*, 164–177.

Meile, C. and P. Van Cappellen. 2003. Global estimates of enhanced solute transport in marine sediments. Limnol. Oceanogr., *48*, 777–786.

Meysman, F. J. R., O. S. Galaktionov, B. Gribsholt and J. J. Middelburg. 2006. Bio-irrigation in permeable sediments: advective pore water transport induced by burrow ventilation. Limnol. Oceanogr., *51*, 142–156.

Meysman, F. J. R., O. S. Galaktionov and J. J. Middelburg. 2005. Irrigation patterns induced in

permeable sediments by burrow ventilation: a case study of *Arenicola marina*. Mar. Ecol. Prog. Ser., *303*, 195–212.

Meysman, F. J. R., J. J. Middelburg, P. M. J. Herman and C. H. R. Heip. 2003. Reactive transport in surface sediments. II. Media: an object-oriented problem-solving environment for early diagenesis. Comput. Geosci., *29*, 301–318.

Oelkers, E. H. 1996. Physical and chemical properties of rocks and fluids for chemical mass transport calculations, *in* Reactive Transport in Porous Media, P. C. Lichtner, C. C. Steefel and E. H. Oelkers, eds., The Mineralogical Society of America, 131–191.

Rasmussen, A. D., G. T. Banta and O. Andersen. 1998. Effects of bioturbation by the lugworm *Arenicola marina* on cadmium uptake and distribution in sandy sediments. Mar. Ecol. Prog. Ser., *164*, 179–188.

Reichardt, W. 1988. Impact of bioturbation by *Arenicola marina* on microbiological parameters in intertidal sediments. Mar. Ecol. Prog. Ser., *44*, 149–158.

Reise, K. 1985. Tidal Flat Ecology, Springer-Verlag, 191 pp.

Rhoads, D. C. 1974. Organism-sediment relations on the muddy sea floor. Oceanogr. Mar. Biol., *12*, 263–300.

Riisgård, H. U. and G. T. Banta. 1998. Irrigation and deposit feeding by the lugworm *Arenicola marina*, characteristics and secondary effects on the environment. A review of current knowledge. Vie Milieu, *48*, 243–257.

Schluter, M., E. Sauter, H. P. Hansen and E. Suess. 2000. Seasonal variations of bioirrigation in coastal sediments: modelling of field data. Geochim. Cosmochim. Acta, *64*, 821–834.

Soetaert, K., P. M. J. Herman and J. J. Middelburg. 1996. A model of early diagenetic processes from the shelf to abyssal depths. Geochim. Cosmochim. Acta, *60*, 1019–1040.

Timmermann, K., G. T. Banta, J. Larsen and O. Andersen. 2003. Modelling particle and solute transport in sediments inhabited by *Arenicola marina*. Effects of pyrene on transport processes. Vie Milieu, *53*, 187–200.

Timmermann, K., J. H. Christensen and G. T. Banta. 2002. Modeling of advective solute transport in sandy sediments inhabited by the lugworm *Arenicola marina*. J. Mar. Res., *60*, 151–169.

Van Cappellen, P. and Y. F. Wang. 1996. Cycling of iron and manganese in surface sediments: a general theory for the coupled transport and reaction of carbon, oxygen, nitrogen, sulfur, iron, and manganese. Am. J. Sci., *296*, 197–243.

Vanderborght, J. P., R. Wollast and G. Billen. 1977. Kinetic-models of diagenesis in disturbed sediments. 1. Mass-transfer properties and silica diagenesis. Limnol. Oceanogr., *22*, 787–793.

Wallmann, K., P. Linke, E. Suess, G. Bohrmann, H. Sahling, M. Schluter, A. Dahlmann, S. Lammers, J. Greinert and N. Von Mirbach. 1997. Quantifying fluid flow, solute mixing, and biogeochemical turnover at cold vents of the eastern Aleutian subduction zone. Geochim. Cosmochim. Acta, *61*, 5209–5219.

Webb, A. P. and B. D. Eyre. 2004. Effect of natural populations of burrowing thalassinidean shrimp on sediment irrigation, benthic metabolism, nutrient fluxes and denitrification. Mar. Ecol. Prog. Ser., *268*, 205–220.

Wenzhöfer, F. and R. N. Glud. 2002. Benthic carbon mineralization in the Atlantic: a synthesis based on in situ data from the last decade. Deep-Sea Res. Part I-Oceanogr. Res. Pap., *49*, 1255–1279.

Received: *31 August, 2005;* revised: *10 March, 2006.*